ACC JOURNAL
XXVI
1/2020

Issue A

Natural Sciences and Technology

INTERNATIONALES
HOCHSCHULINSTITUT
ZITTAU

ZENTRALE WISSENSCHAFTLICHE
EINRICHTUNG DER TU DRESDEN

Uniwersytet Ekonomiczny
we Wrocławiu

Indexed in:

INDEX COPERNICUS

I N T E R N A T I O N A L

Liberec – Zittau/Görlitz – Wrocław/Jelenia Góra

ACC JOURNAL je mezinárodní vědecký časopis, jehož vydavatelem je Technická univerzita v Liberci. Na jeho tvorbě se podílí čtyři vysoké školy sdružené v Akademickém koordinačním středisku v Euroregionu Nisa (ACC). Ročně vycházejí zpravidla tři čísla.

ACC JOURNAL je periodikum publikující původní recenzované vědecké práce, vědecké studie, příspěvky ke konferencím a výzkumným projektům. První číslo obsahuje příspěvky zaměřené na oblast přírodních věd a techniky, druhé číslo je zaměřeno na oblast ekonomie, třetí číslo pojednává o tématech ze společenských věd. ACC JOURNAL má charakter recenzovaného časopisu. Jeho vydání navazuje na sborník „Vědecká pojednání", který vycházel v letech 1995-2008.

ACC JOURNAL is an international scientific journal. It is published by the Technical University of Liberec. Four universities united in the Academic Coordination Centre in the Euroregion Nisa participate in its production. There are usually three issues of the journal annually.

ACC JOURNAL is a periodical publishing original reviewed scientific papers, scientific studies, papers presented at conferences, and findings of research projects. The first issue focuses on natural sciences and technology, the second issue deals with the science of economics, and the third issue contains findings from the area of social sciences. ACC JOURNAL is a reviewed one. It is building upon the tradition of the "Scientific Treatises" published between 1995 and 2008.

Contents

Research Articles

Research Articles

EXPERIMENTAL STUDY OF THE PERFORMANCE OF BASE METAL AND WELDING LINE OF THE HOUSEHOLD L. P. G. CYLINDERS MANUFACTURED IN KURDISTAN REGION

Yassin Mustafa Ahmed[1]; **Hameed D. Lafta**[2]; **Azhin Abdullah Abdul Rahman**[3]; **Barzan Talib Salih**[4]

Sulaimani Polytechnic University,
Technical College of Engineering, Department of Mechanical Engineering
Sulaimani, Kurdistan region, Iraq
e-mail: [1]yassin.ahmed@spu.edu.iq; [2]hameed.lafta@spu.edu.iq;
[3]azhinabdullah92@gmail.com; [4]barzan69@gmail.com

Abstract

Liquefied petroleum gas (propane or butane) is a colorless liquid which readily evaporates into a gas. It has no smell, although it will normally have an odor added to help detect leaks. Liquefied petroleum gas is stored and handled as a liquid when under pressure inside an LPG cylinder. Liquefied petroleum gas cylinders are subjected to various tests to ensure their compliance requirements as per standard. This research studies the durability of welding and performance of base metal of L. P. G. home cylindrical in Kurdistan region. The experiments were carried out on three types of LPG cylinders used in Kurdistan regions: A, B, and C and an unformed plate. To carry out the samples and tests during the research, we relied on the standard tests for LPG cylinders. Three samples are extracted from each of LPG cylinders and an unformed plate for each of tensile test, Bending test and Hardness test according to ISO 6892-2016 and ASME standards from each type of LPG cylinders and from unformed plate to examine the mechanical properties. In addition, chemical compositions were also carried out. These values are compared with the standard.

Keywords

LPG; ASTM; ASME; ISO; BS 5045.

Introduction

Liquefied Petroleum Gas (LPG) is a colorless liquid which readily evaporates into a gas. It has no smell, although it will normally have an odor added to help detect leaks. When mixed with air, the gas can burn or explode when it meets a source of ignition. It is heavier than air, so it tends to sink towards the ground [1]. LPG is composed predominantly of a mixture of hydrocarbons such as propane, propylene, butane or butylene. The gas can be liquefied at moderate pressure, and can be stored in cylinders as a liquid under pressure and is drawn out and used as gas. This means that it can be transported and stored as liquid and burnt as gas. The expansion ratio of gas liquid is 270:1 at atmospheric pressure. The expansion factor makes LP-gas more economical to be transported and stored with large quantities of gaseous fuel in a small container. Containers are normally filled by 80-85% liquid, leaving 15-20% vapor space for expansion due to temperature increase. The household gas cylinder weighs approximately 14 kg. Nowadays, composite materials have been used widely, which is proved to be more effective. These composite materials are wound over metal liner thus acting as an over wrapped composite pressure vessel. LPG cylinder is one kind of a pressure vessel that stores pressurized gases. LPG cylinder material should have high tensile and compressive

strength for withstanding the high pressure of the gases [2]. The Cylinders play a crucial role in containing and transporting hazardous LPG from the filling plant to the end consumer [3].
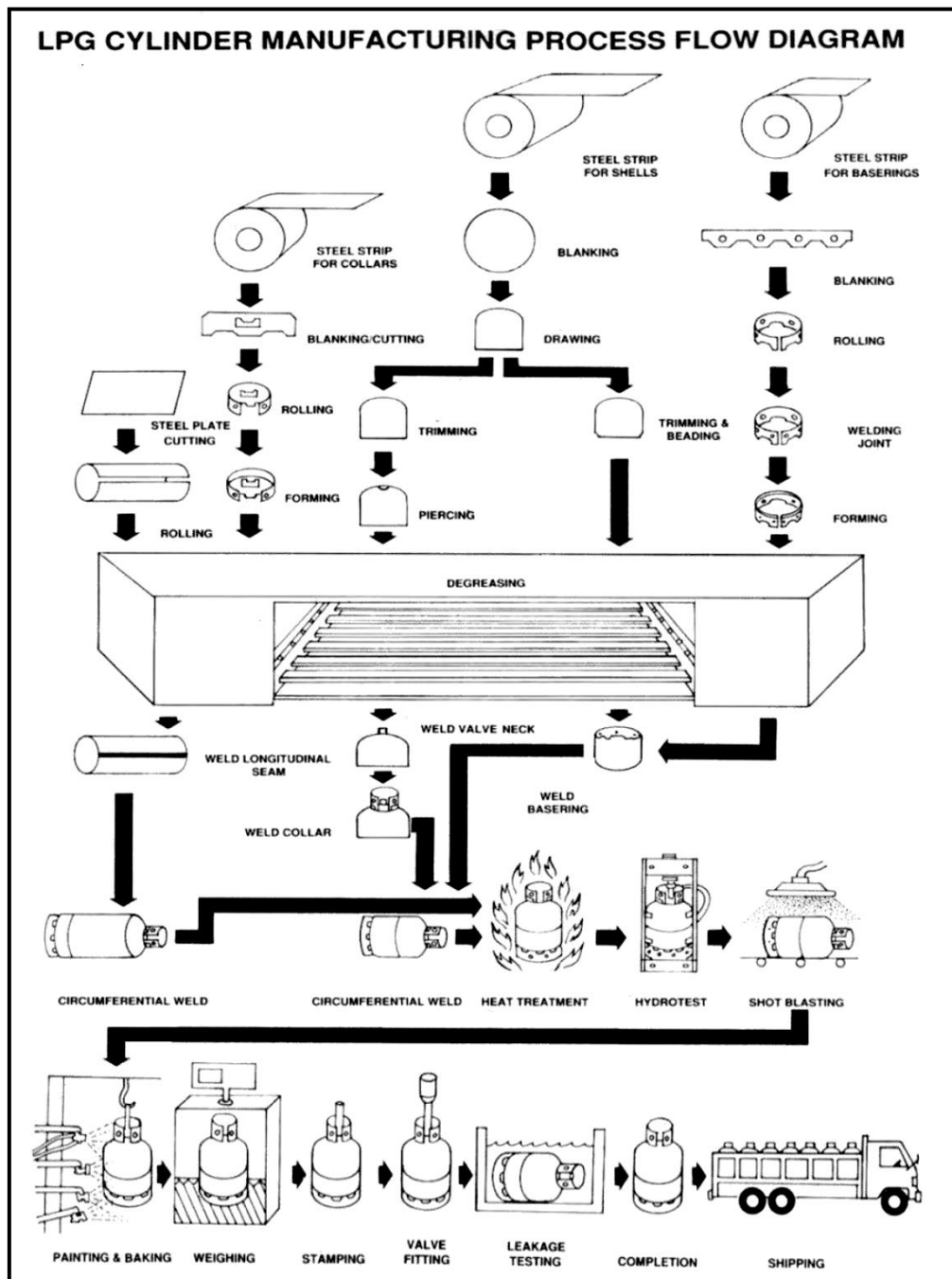
Source: [5]
Fig. 1: *The process of manufacturing of LPG cylinders*

LPG Cylinders are to be manufactured from definitely prescribed raw material to ensure safety of cylinders through material quality specifications [4]. Although there are clear standards and statutory norms for design, manufacturing and usage of cylinders, there are certain gaps in these standards in terms of ensuring material safety compliance. LPG cylinder production is composed of several sheet metal forming, surface treatment and testing processes. The process starts with blanking, deep drawing and piercing, trimming and joggling. Next are the welding operations for valve boss, valve guard ring, foot ring and the two halves. The finished cylinder is then heat treated, tested, shot blasted, painted and then the

valve is attached and tested finally [5]. The main steps involved in manufacturing process of LPG cylinders are shown in Fig. 1.

1   Literature Review

Liquefied petroleum gas (LPG) cylinders that have an important position from the point of use have been taken into consideration, therefore, as explained below, intensive research has been carried out by the researchers Siddiquia, Ramakrishna and Lalc [6] who investigated a study on the welded low-carbon steel cylinders exceeding 5 liters of water capability which was produced and tested as per Indian Standard (IS 3169).

Lalc, Ramakrishna and Siddiquia [7] conducted several tests on LPG cylinders, in which the acceptance test is one of the most important tests to reveal cylinder parent metal mechanical properties. Two tensile specimens are prepared from finished cylinder batch for this test and tested on a universal testing machine to determine yield strength, percentage elongation and ultimate tensile strength of parent metal. Values of these test results are compared to standard values prescribed in Indian standards to decide acceptance of cylinder batch for market release.

Mahmud et al. [8] have studied the effect of annealing temperature on the mechanical properties of SG 255 steel. The SG 255 steel is used in manufacturing of domestic LPG cylinder in Kurdistan region. Furthermore, their work aims to obtain experimentally better mechanical properties at particular ductility with lower annealing temperature and to minimize the cost of the manufacturing of LPG cylinders. A number of samples were made according to ISO 6892, and then heat treated with different annealing temperature (850, 900, and 950 ºC). Moreover, the tensile tests of these samples were carried out until failure to obtain the mechanical properties. It was shown that higher elongation percentage 34.18% with an annealing temperature of 900 ºC can be achieved, and this leads to minimizing the cost of manufacturing of the cylinders without degrading their quality.

Li et al. [9] proposed an integral manufacturing process with hot drawing and cold flow forming for large diameter seamless steel gas cylinders. The primary aim of this research was to find out the impacts of the manufacturing method on gas cylinders made of 34CrMo4 steel's microstructure and mechanical characteristics. Two preformed cylinders were produced by hot drawing. One cylinder was then further manufactured by cold flow forming. The experiments were carried out using three types of material samples, namely base material (BM), hot drawing cylinder (HD), and cold flow-formed cylinder (CF). Tensile and impact tests were performed to examine the mechanical properties of the cylinders in longitudinal and transverse directions. Microstructure evolution was analyzed by scanning electron microscopy (SEM) and electron backscatter diffraction (EBSD) to reveal the relation between the mechanical properties and the microstructure of the material. It was found out that the mechanical properties of the 34CrMo4 steel gas cylinders were significantly improved after hot drawing and flow forming plus a designed heat treatment, compared with the base material. The observations of microstructure features such as grain size, sub grain boundaries, and residual strain support the increase in mechanical properties due to the proposed manufacturing process.

2   Research Subject

In this study, an unformed plate and the sheet materials of liquefied petroleum gas (LPG) cylinders that have an important position from the point of use have been taken into consideration. The household LPG cylinders can be divided into two main groups, the first group imported by the central government and the second group locally produced in the

Kurdistan region by different companies and in different cities. A group of specimens was taken from the unformed plate and base metal of the cylinders, while other ones were taken across the cylinders from the weld zone transversely in the middle of the cylinders, which had the same initial thickness of 3 mm. It is worth mentioning that the effect of geometric discontinuities due to weld toe was eliminated since the thickness of entire samples was kept constant. Different test results are compared to the standard.

3   Methodology

3.1   Materials

The material of the LPG cylinders and unformed plate is low alloy carbon steel with 3mm thickness. The mechanical and chemical composition required according to BS 5045 [10] is given in Tables 1 and 2 respectively.

Tab. 1:   *Mechanical properties of LPG cylinders*

Mechanical properties of LPG cylinders	Value
Minimum yield strength	240 N/mm^2
Tensile strength	360-430
Minimum elongation	30 %

Source: [10]

Tab. 2:   *Chemical composition of LPG cylinders*

Chemical composition	% max
C	0.16
Mn	0.50
Si	0.20
P	0.03
S	0.03

Source: [10]

3.2   Chemical Composition Analysis

To achieve this study, we used three LPG cylinders from different companies and different cities (B, C, D) and an unformed plate (A) to make the specimens. To distinguish between the LPG cylinders, and also to mention the name of the companies or cities, different letters are used. The letter (A) indicates the unformed plate, (B) is the letter used for the first cylinder, (C) is the letter for the second cylinder, and (D) is the letter for the third cylinder. The chemical compositions examination of the test specimens were achieved by spectrometry instrument, see Fig. 2.

Fig. 2: *Chemical composition of samples*

The results of chemical composition are shown in Table 3.

Tab. 3: *Chemical composition of LPG cylinders and unformed plate*

Sample	C %	Si %	Mn %	P %	S %
A	0.129	0.192	0.92	<0.0005	<0.0005
B	0.119	0.082	1.05	<0.0005	0.0054
C	0.135	0.163	0.926	0.0005	0.0030
D	0.124	0.181	0.966	<0.0005	0.0034

From the above-mentioned chemical compositions of cylinders and unformed plate, it can be seen in Table 3 that the contents of all elements, except for silicon and manganese in all samples were nearly the same. Sample (B) had a lower silicon content and higher manganese content than the other samples, since all cylinders came from different production batches and thus were likely to be from different raw steel sheet. With respect to the investigations of this work, these small deviations could be neglected. However, all the chemical contents of all cylinders and the unformed plate were in the acceptable range of the standard of steel grades used for LPG cylinder except manganese.

3.3 Tensile Test

The investigated LPG cylinders were manufactured by using deep drawing process from two low-carbon steel plates with a dome shape and an intermediate cylinder, which were subsequently welded together along the peripheral direction, see Fig. 1. Microstructure and mechanical behavior of the welding line were differed from the base low carbon steel and could considerably affect the structural integrity and performance of the LPG cylinder. Tensile testing was carried out at a room temperature of 23 °C as per ISO 6892-2016 [11]. The tensile test specimens with the gauge length of 50 mm were prepared from the sidewall of cylinders in the longitudinal direction. A group of specimen was taken from the base metal, while another one was taken across the cylinders and had the weld zone transversely in the middle according to ASME section IX 2013 [12], as shown in Fig. 3 and 4.

Fig. 3: *Tensile test samples (weld metal)*

Fig. 4: *Tensile test samples (base metal)*

Fig. 5: *Tensile test machine*

Note that the effect of geometric discontinuities due to weld toe was eliminated since the thickness of entire samples was kept constant. The tensile tests were carried out on a universal testing machine as shown in Fig. 5.

The achieved mechanical properties such as yield strength, tensile strength and elongation of the base metal and weld area of the specimens were presented in Tables 4 and 5.

Tab. 4: *The tensile test results of the cylinders and unformed plate (base metal)*

Sample	Ultimate strength (MPa)	Yield strength(MPa)	Elongation
A	456.86	325.56	33.80
B	389.86	249.33	28.80
C	417.20	283.33	25.90
D	447.40	304.00	28.53
Standard	(360-430)	min (240)	Min (30)%

Source: Own

By observing the tensile test results, we found out that the unformed metal (sample A) and sample (D) exhibited highest yield and tensile strengths whereas sample (B) had lower ultimate and yield strength while its elongation was similar to sample (D) and higher than of sample (C). Furthermore, the yield and tensile strengths of sample (C) were greatly higher than those of sample (B) while the elongations of sample (c) much decreased as compared to sample (A). It is obvious that the tensile properties especially the elongation of sample B, C, D were little different from BS 5045 standard [10] and the yield stress is higher than 240 MPa in all cases; all gas cylinders are within the range of BS 5045 standard [10], however, the ultimate strength of sample (A), (D) is greater than that of the standard as shown in Table 4. It can be concluded that the subsequent forming process does not cause significant changes in the mechanical properties of the material after heat treatment.

Tab. 5: *The tensile test results of the cylinders on welded area*

Sample	Ultimate strength (MPa)	Yield strength(MPa)	Elongation
B (tensile shear strength)	361.9	306	47.8
B (ASME)	405.5	310	28.3
C (ASME)	447.8	310	35.0
D (ASME)	434.7	305	35.5
Standard	(360-430)	min (240)	Min (30)%

Source: Own

On the other hand, from Table 5 it can be seen that the sample (C) and the sample (D) exhibited high ultimate tensile strengths and yield strength with similar elongation whereas sample (B) had lower ultimate tensile shear strength while its elongation was higher than of those samples. Furthermore, the elongation of sample (B) was much lower than those of the other samples. It is obvious that the tensile properties, especially the elongation of sample B, C, and D, were little different from BS 5045 standard [10] and the yield stress is higher than 240 MPa in all cases; all gas cylinders are within the range of BS 5045 standard [10]; however, the ultimate strength of sample (A), (D) is greater than that of the standard, as shown in Table 5. It is apparent that the material of the cylinders exhibits good ductility.

3.4   Hardness Test

The preparation of hardness test samples has been carried out with an appropriate cutting method, which involves selecting the correct cutting tool and using a cooling liquid to avoid the samples from burning and distortion. To cut and prepare the specimens for the hardness exam, a milling machine process with cooling liquid was used, see Fig. 6.

Fig. 6: *Cutting process of LPG cylinders*

After cutting, the samples were grinded and polished in order to prevent any scratches and to accomplish right reading. The Vickers hardness testing was carried out for different locations of the sample face to check the consistency and uniformity of the properties, see Fig. 7. The micro-hardness testing was carried out as per ASTM E384 [13] standard. Diamond indenter (pyramid) with face angle of 136° was used. During testing 1 kg load was applied on sample with dwell time of 15 seconds, and both the diagonals of pyramid indenter (d1 and d2) were measured with a microscope at a magnification of 500X.

Fig. 7: *Hardness test samples*

The results of the hardness tests have shown in Table 6 and Fig.8 respectively.

Tab. 6: *Results of the average hardness test*

Sample	Average Vickers hardness (kg/mm^2)
Sample (A)	147.24
Sample (B)	153.28
Sample (C)	142.70
Sample (D)	162.66
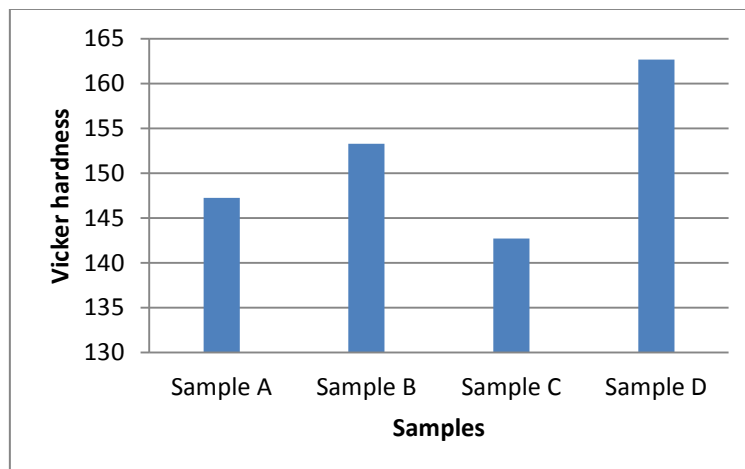
Fig. 8: *The diagram of the Results of the hardness test of samples*

The average hardness results revealed that the values of (sample D) offered the highest value as compared to other samples while sample (C) shows the lower result as compared to others.

3.5   Bending Test

Bending test is a one of important tests that standard required to achieve. This test achieved perpendicular to the weld zone which has been bent through the angle of 180°. Bending tests for ductility provide a simple way to evaluate the quality of materials by their ability to resist cracking or other surface irregularities during one continuous bend condition. The bending tests were carried out in accordance with AWS standard [14] for all three LPG cylinders to evaluate their welding qualities. The results of such a test obtained by the same tensile machine, the bending test samples and machine are shown in Figures 9, 10, and 11.

Source: Own
Fig. 9: *Prepared bending test samples*

Source: Own
Fig. 10: *Bending test sample*

Source: Own
Fig. 11: *Bending test machine*

The bending test results showed that the samples were bent at 180 degrees without breaking or cracking in the samples. This means that the samples met the requirements of the standards. The ductility of weld was satisfactory and there are no defects in the welding joints for all samples.

Conclusion

Based on the results of tensile, hardness, bending tests, and chemical composition results of the current study it can be concluded that all the chemical contents of all cylinders and an

unformed plate were in the acceptable range of the standard of steel grades used for LPG cylinder except manganese. In addition, the tensile properties of the unformed plate and base metal of the LPG cylinders were show little different from BS 5045 standard [10] and they are in the acceptable range. On the other hand, the ultimate tensile strength, yield strength and elongation of the weld metal of the LPG cylinders are nearly similar according to ASME standard. For the hardness test it is clear from the results that the average hardness values of sample (D) have recorded greatest value when compared with other samples. It can also be seen that the bending results showed that no development of crack was noticed during the bending test.

Literature

[1]   TRIPATHI, A.; KUMAR, A.; CHANDRAKAR, M.: Design and Analysis of a Composite Cylinder for the Storage of Liquefied Gases. *International Journal for Scientific Research & Development*. 2017, Vol. 5, Issue 3, pp. 871–876. Online ISSN 2321-0613.

[2]   KIRAN, C. S.; SRUTHI, J.: Design and Finite Element Analysis of Domestic LPG Cylinder using ANSYS Workbench. *CVR Journal of Science and Technology*. 2018, Vol. 14, pp. 97–101. ISSN 2277-3916. DOI: 10.32377/cvrjst1419

[3]   NIYAMAT, M.; BICHA, K.: Design and Stress Analysis of Pressure Vessel by Using ANSYS. *International Journal of Engineering Sciences & Research Technology*. 2015, Vol. 4, Issue 7, pp. 578–585. ISSN 2277-9655.

[4]   RAMAKRISHNA, A.; SIDDIQUIA, N. A.; LALC, P. S.: Review of Liquefied Petroleum Gas (LPG) Cylinder Life Cycle. *International Journal of Advanced Engineering Technology*. 2013, Vol. 4, pp. 124–127.

[5]   BUREAU OF INDIAN STANDARDS: *Product Manual for Hot Rolled Steel Plate (up to 6mm), Sheet and Strip for the Manufacture of Low Pressure Liquefiable Gas Cylinders according to IS 6240:2008*. [online]. 2020. Available from WWW: http://bis.gov.in/wp-content/uploads/2020/02/PM_IS_6240.pdf

[6]   SIDDIQUIA, N. A.; RAMAKRISHNA, A.; LALC, P. S.: Review on Liquefied Petroleum Gas Cylinder Acceptance Test as per Indian Standard, IS 3196 (Part 3): 2012. *International Journal of Advanced Engineering Technology*. 2013, Vol. 4, pp. 119–123.

[7]   LALC, P. S.; RAMAKRISHNA, A.; SIDDIQUIA, N. A.: Impact of Sample Preparation Methods on Liquefied Petroleum Gas Cylinder Parent Metal Tensile. *Journal of Engineering Research and Studies*. 2013, pp. 12–15.

[8]   MAHMUD, F. J.; ABDULRAHMAN, K. M.; MUHAMMED, H. J.; SEED, B. A. H.: The Influence of Annealing Temperature and Soaking Time on the Ductility of SG 255. *Kurdistan Journal of Applied Research*. 2017, Vol. 2, Issue 3. Print ISSN 2411-7684. Electronic ISSN 2411-7706. DOI: 10.24017/science.2017.3.60

[9]   LI, Y.; FANG, W.; LU, Ch.; GAO, Z., MA, X.; JIN, W.; YE, Y.; WANG, F.: Microstructure and Mechanical Properties of 34CrMo4 Steel for Gas Cylinders Formed by Hot Drawing and Flow Forming. *Materials*. 2019, Vol. 12, Issue 8. DOI: 10.3390/ma12081351

[10] BRITISH STANDARDS INSTITUTION: *BS 5045-2:1978. Specification for transportable gas containers. Steel containers up to 130 litres water capacity with welded seams*. [online]. 1978. Available from WWW: https://shop.bsigroup.com/ProductDetail/?pid=000000000010100408

[11] ISO: ISO 6892-1:2016. *Metallic materials — Tensile testing — Part 1: Method of test at room temperature*. [online]. 2016. Available from WWW: https://www.iso.org/standard/61856.html

[12] ASME: *ASME Boiler and Pressure Vessel Code*. Section IX. [online]. 2013. Available from WWW: https://www.browntechnical.org/content/PDF/ASME BPVC-IX-2013.pdf

[13] ASTM: *ASTM E384 – 11. Standard Test Method for Knoop and Vickers Hardness of Materials*. [online]. 2011. DOI: 10.1520/E0384-11

[14] AMERICAN WELDING SOCIETY: *Welding Handbook, Volume 1, Welding and Cutting Science and Technology*. 10th Edition. AWS, 2018. Print ISBN 978-1-64322-014-7. PDF ISBN 978-1-64322-015-4.

Dr. Yassin Mustafa Ahmed; Dr. Hameed D. Lafta; Azhin Abdullah Abdul Rahman, BSc; Barzan Talib Salih, BSc

EXPERIMENTÁLNÍ STUDIE VÝKONNOSTI ZÁKLADNÍCH KOVŮ A SVAŘOVACÍ LINKY LPG LAHVÍ POUŽÍVANÝCH V DOMÁCNOSTECH V KURDISTÁNU

Zkapalněný ropný plyn (propan nebo butan) je bezbarvá kapalina bez zápachu, která se snadno vypaří na plyn. Pro detekci netěsnosti bývá aromatizována. Zkapalněný ropný plyn je skladován a zpracováván jako kapalina pod tlakem uvnitř tlakových lahví, které jsou testovány, zda odpovídají normě.

Výzkum se zabývá trvanlivostí svařování a provedením základního kovu u lahví používaných v domácnostech v Kurdistánu. Pokusy byly prováděny na třech typech standardních lahví a na netvarované desce. Z každé tlakové lahve a z netvarované desky se odeberou tři vzorky pro zkoušku tahem, ohybem a zkoušku tvrdosti podle norem ISO 6892-2016 a standardy ASME včetně analýzy chemického složení. Získané hodnoty jsou porovnány se standardem.

EXPERIMENTELLE STUDIE ZUR LEISTUNGSFÄHIGKEIT VON GRUNDMETALLEN UND ZUR SCHWEISSLINIE VON LPG-FLASCHEN, WIE SIE IN HAUSHALTEN IN KURDISTAN VERWENDUNG FINDEN

Verflüssigtes Erdölgas (Propan oder Butan) ist eine farb- und geruchlose Flüssigkeit, welche leicht in den gasförmigen Zustand übergeht. Zur Detektion von Undichtigkeiten wird sie aromatisiert. Das verflüssigte Erdölgas wird als Flüssigkeit unter Druck in Druckflaschen gelagert, welche getestet werden, ob sie der Norm entsprechen.

Die Untersuchung befasst sich mit der Haltbarkeit des Schweißens und der Ausführung des Grundmetalls bei den Flaschen, wie sie in Haushalten in Kurdistan verwendet werden. Die Versuche wurden an drei Typen von Standardflaschen und an der ungeformten Platte durchgeführt. Jeder Druckflasche und jeder ungeformten Platte werden drei Proben entnommen für einen Versuch zur Zug- und Biegungsfestigkeit sowie für eine Härteprobe gemäß den Normen ISO 6892-2016 und für den Standard ASME inklusive einer Analyse der chemischen Zusammensetzung. Die dabei gewonnen Werte werden mit dem Standard verglichen.

EKSPERYMENTALNE BADANIE WYDAJNOŚCI PODSTAWOWYCH METALI I LINII SPAWALNICZEJ BUTLI LPG UŻYWANYCH W GOSPODARSTWACH DOMOWYCH W KURDYSTANIE

Skroplony gaz ropopochodny (propan lub butan) to bezbarwna, bezzapachowa ciecz, która łatwo odparowuje w gaz. W celu wykrycia nieszczelności bywa aromatyzowana. Skroplony gaz ropopochodny magazynowany i przetwarzany jest jako ciecz pod ciśnieniem w butlach gazowych, które są testowane pod kątem spełnienia normy.

Badania dotyczą trwałości spawania i wykonania podstawowego metalu w przypadku butli używanych w gospodarstwach domowych w Kurdystanie. Badania przeprowadzano na trzech typach standardowych butli oraz nieformowanej płycie. Z każdej butli gazowej i nieformowanej płyty pobierane są trzy próbki do badania poprzez ciągnięcie, zginanie i badania twardości wg norm ISO 6892-2016 oraz standardów ASME wraz z analizą składu chemicznego. Uzyskane wartości porównywane są ze standardem.

RESEARCH AND DEVELOPMENT OF AN ARTIFICIAL NEURAL NETWORK FOR SPECTRAL DATA

Theo Dedeken
Ghent University, Faculty of Sciences, Krijgslaan 281, 9000 Ghent, Belgium
e-mail: theo.dedeken@telenet.be

Abstract

There is a global call to determine the state of the inventory of transport and storage containers for high radioactive waste (spent fuel assemblies). One possible solution is to perform vibration analyses and evaluate vibration responses by using artificial neural networks. For this approach, first investigations have been carried out. Vibration data are obtained from a testing setup modelling the nuclear storage fuel assemblies which is converted to the frequency domain via the Fourier transform. Raw spectral data are first prepared by normalization, data augmentation and limiting the frequency range. These measures are proven to have significant impact on the overall performance of the training of the neural networks. Using fully connected and convolutional neural networks, classification and regression is performed on the spectral data. Classification is shown to be possible with very high accuracy; and regression has decent results with options for improvement in later stages. Convolutional neural networks are shown to be superior in both cases.

Keywords

Neural networks; Spectral data; Nuclear waste monitoring; Vibration analysis.

Introduction

The storage of nuclear waste is a complex and worldwide problem. Currently there are little to none long term solutions available for storing spent fuel assemblies, hence the waste is stored in intermediate transport and storage containers inside the nuclear power plants. These storage containers require active maintaining and monitoring to avoid dangerous and environmentally damaging situations.

To research and develop novel solutions to these problems, a cooperative project was set up between Dresden Technical University (TUD) and Zittau/Görlitz University of Applied Sciences (HSZG). In light of this project different possible non-invasive measurement principles were proposed [1]. This paper focuses on the monitoring of containers using vibration analysis and training neural networks on the obtained spectral data to perform classification and assessment of the current state of the storage container inventory.

1 Research Objectives

The aim of the research is to develop novel machine learning solutions for the monitoring of nuclear waste containers. Specifically, by analyzing the vibrations and the resulting spectral decomposition of these signals. To achieve this, a number of neural networks were constructed and trained on the spectral data to predict the state of the waste containers. Additionally, a data augmentation workflow was built and evaluated to increase the effectiveness of the limited amount of data available.

2   Methods

2.1   Data Acquisition

To train a neural network, first a sufficient amount of data needs to be collected. To acquire the data necessary for further research, a testing setup was developed and measurements were performed.

Scale models representing the actual fuel assemblies contained in the storage containers were constructed. The model is assembled as a collection of 16 tubes arranged in a four by four pattern. It is possible to change the amount of filament in these tubes. In this way, a number of different states were constructed; each with a different configuration.

Two main rounds of experiments were performed: the first round with five different states ranging from full to empty. In Fig 1, the configured states for this round are shown. Later, the amount of states was increased to a total of 15. The results presented in section 3 use the data obtained from the last set of experiments.
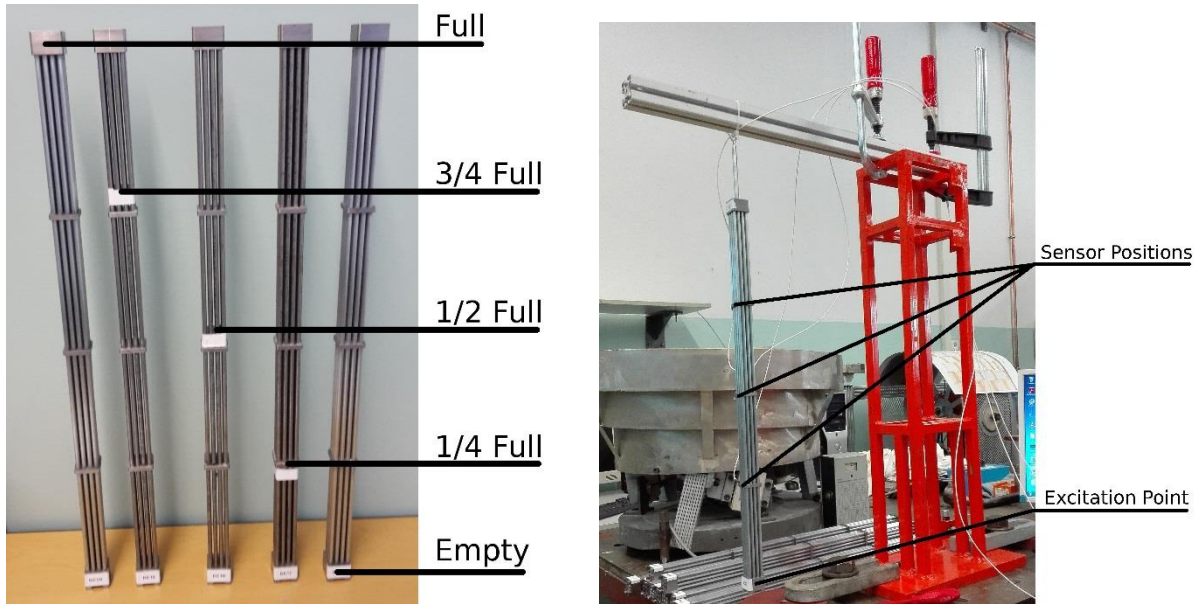
Source: Own
Fig. 1:   *The prepared states for the first round of experiments*

To measure the vibrations on the fuel assembly models, a testing rig was set up where the model could be suspended in the air; this setup is presented in Fig 1. At three positions on the model sensors were attached to register the velocity of that position over time. The three sensors are positioned along the same axis where the impact is occurring. To perform the measurement, an impact hammer was used to hit the assembly. The resulting vibrations were then registered and normalized according to the vibrations measured on the hammer. This process was repeated ten times for each state.

2.2   Data Preparation

The raw data acquired from the sensors are not in a format that is useful for analysis and classification using neural networks. To capture the unique properties of each signal better, we decompose the time series in the frequency domain using the Fourier transform. This leaves us with the frequency values in between 0 Hz and 2000 Hz (Fig 2).
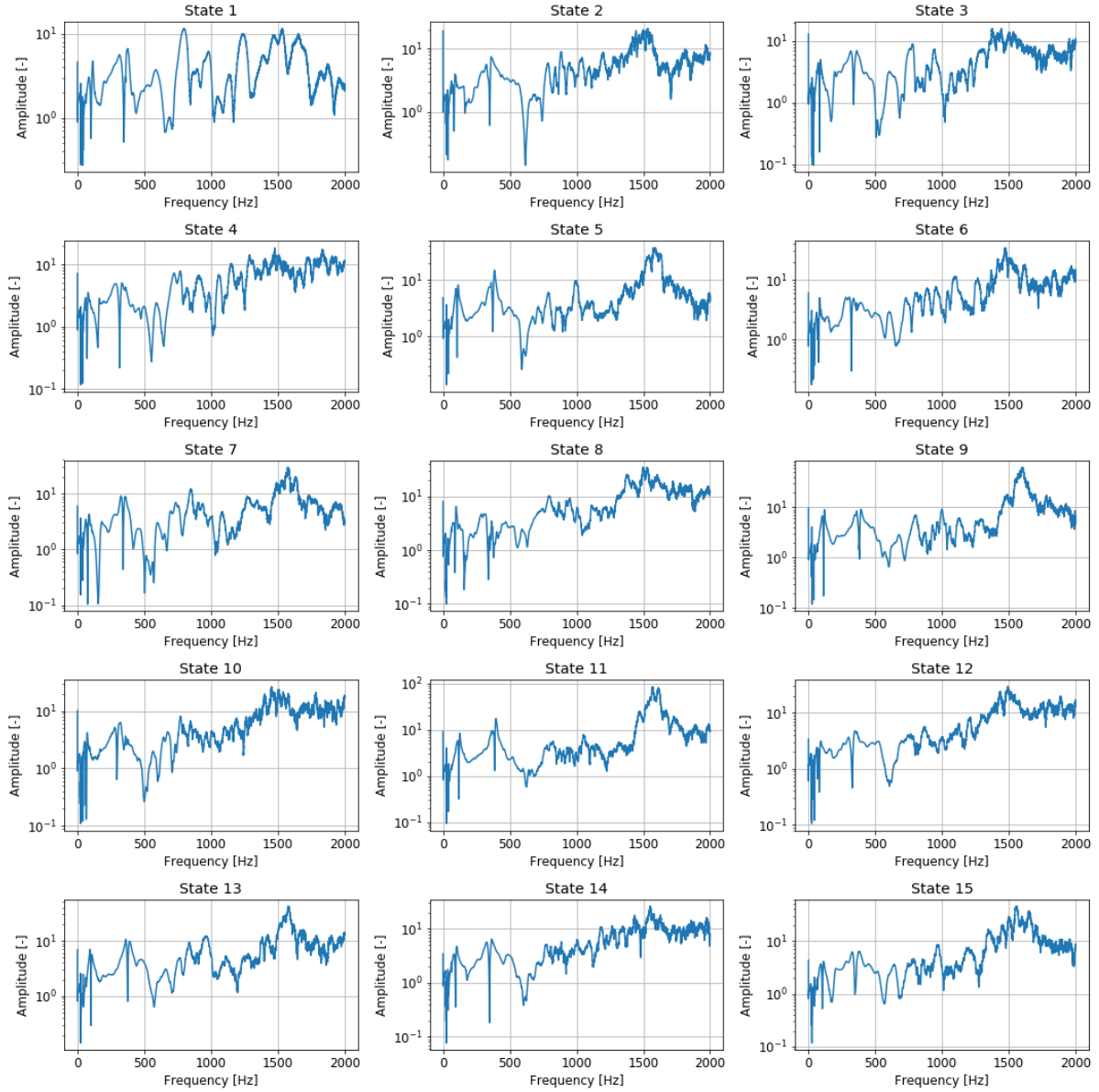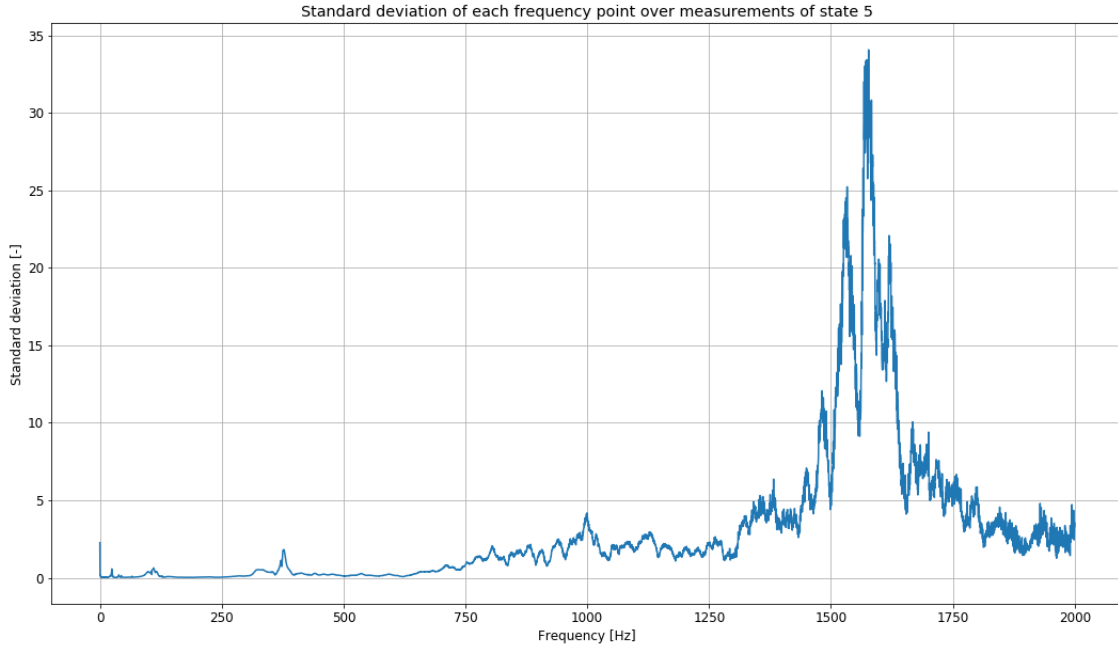
Source: Own

Fig. 2: *All obtained frequency domains for the second round of experiments*

2.2.1 Removing Noise

When looking closer at the variance of the calculated amplitude of each frequency over measurements of the same state (Fig 3), it becomes clear that there are two zones in the spectrum with variance of different magnitude. The calculated amplitudes of the frequencies ranging from 0 Hz to 700 Hz are highly similar in over multiple measurements of the same state. The higher frequencies are exceptionally dissimilar over measurements of the same state. This increase in variance can be mainly attributed to noise caused both by measurement inaccuracies and outside factors.

When training a neural network on samples which are very different but still map to the same output, we run into problems where the network has difficulties to converge to a state that can handle each case of input. Keeping in mind the construction of the spectral domain, we can assume that most of the original vibration data are defined by the values of the lower frequencies. To help the training performance of the used models, we limit the frequency range to the interval [0 Hz, 800 Hz].

Source: Own
Fig. 3: *Variance of the amplitude for each frequency over measurements of the same state*

2.2.2 Data Normalization

Another technique used to improve training performance of the neural networks was to normalize the input data. This was achieved by subtracting the mean value of the spectrum to each value and dividing by the standard deviation afterwards to obtain a data sample with mean zero and standard deviation of one.

2.2.3 Data Augmentation Techniques

Since there were only ten measurements for each state, the amount of the data to train the neural networks on was very limited. To improve the performance and robustness of the network, data augmentation inspired by previous work in [2] were added. The techniques employed in this case were adding an offset to the original spectrum and multiplication of the spectrum. Offset was varied over ±0.1 times the standard deviation of the original sample and multiplication was varied over 1±0.1 times the standard deviation. For each sample, nine extra samples were constructed: three using the offset technique, three using multiplication and three using the combination. This effectively increased the size of our dataset with a factor of ten. It is important to note that the augmentation was executed after the normalization of the data, otherwise the normalization operation would have converted the extra samples back to the original sample.

2.3 Used Models

Training was performed on the two most used variants of feed-forward neural networks, the standard fully connected and convolutional neural networks. An architecture of comparable complexity for each one of the variants was constructed and trained on the prepared spectral data. See section 3.1 for the comparison of different models.

The networks were constructed in the Keras [3] framework using the Tensorflow [4] backend. As for the optimizer, an instance of the Adam optimizer was used, configured with a learning rate of 0.0001.

2.3.1 Fully Connected Neural Network

The fully connected network shown in Fig 4 consists of an input layer, two hidden layers and the output layer. The hidden layers have 256 neurons and are combined with the Exponential Linear Unit (ELU) activation function and a dropout measure dropping out 25% of the inputs.

The depth of the neural network was kept small as increases in layers did not cause any major improvements in performance of the network. The ELU activation function has good training performance as it does not have the same problems with vanishing gradient compared to the sigmoid activation function. Dropout is added as a measure to make the resulting network more robust and prevent overfitting of the data.
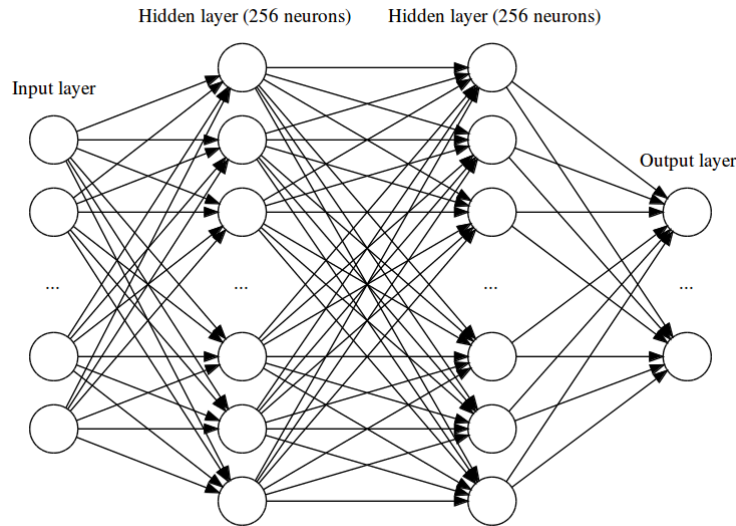
Source: Own
Fig. 4: *Fully connected neural network architecture*

2.3.2 Convolutional Neural Network

The convolutional neural network shown in Fig 5 consists of an input layer, three convolutional layers, one hidden layer and the output layer. The three convolutional layers have 32, 64 and 128 kernels respectively. After each of the convolutional layers, a max pooling operation is performed with pool size of three. At the end of these layers the input space is reduced sufficiently to be fully connected to a single hidden layer with ELU activation and a dropout measure with a dropout rate of 25%.
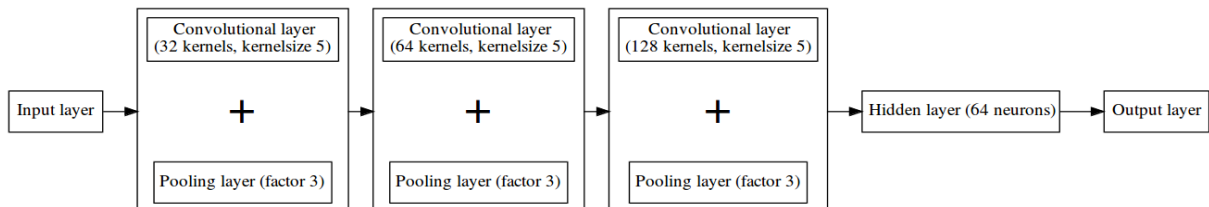
Source: Own
Fig. 5: *Convolutional neural network architecture*

2.4 Training Input

In the case of the fully connected network, the input of the network is constructed by concatenating the spectra after data preparation of the three positions. Each amplitude value in the resulting array then serves as an input node to the neural network.

As far as the convolutional neural network is concerned, a different approach can be used. Since convolutional neural networks work on volumes rather than single input nodes, we can construct the input as a two dimensional array by stacking the spectra of each position. This resembles the way convolutional neural networks are used in the case of colour images where each image pixel has three components, one for each of the colour channels.

To make sure the model was generalizing well, a validation split of 0.5 was chosen. This meant that only half of the samples were used in the training of the network. With the addition of data augmentation, the models still had sufficient data to be trained on.

2.5 Output Encoding

Two different types of encoding were used for the expected output for the networks, each of them more appropriate in different approaches of solving this problem.

2.5.1 One-Hot Encoding

To convert the state number to this encoding, an *n*-dimensional vector was constructed (*n* being the number of states: 5 or 15). In this vector, all elements are zero except for the element at the position of the state being encoded.

This encoding was used to train the networks to perform a classification of the input sample. A property of this encoding is that we can interpret the output as a distribution of how confident the network is about its prediction: the more confident, the more the input will resemble the one-hot encoding. If multiple positions in the output are high, we can presume that the network recognizes properties from both states in the input. To get the output in the desired format, a softmax activation layer was added as the last layer of the models. With this output format, the categorical cross entropy between the expected output and the actual output was used as the loss measure while training.

2.5.2 Continuous Value

Another way to encode the state of a particular sample is to use a single value. In this case, the state number is converted to a number in the range [0, 1]. This is done by linearly interpolating the states number to the new range.

This encoding was used when solving this problem as a regression one. As the states are numbered 1-15 going from empty to full, we can interpret the output as a value representing the amount of filling in the assembly. To limit the range of the output of the neural network model, a sigmoid activation layer was added as the last layer of the model. With this output format, the mean squared error between the expected output and the actual output was used as the loss measure while training.

3 Results

3.1 Comparison of Used Models

3.1.1 Classification

The evolution of the accuracy and loss function during training for each of the models is presented in Fig 6. It is clear that the convolutional model achieves the best performance in both categories. However, it is important to note that the training of the convolutional generally requires double the time per training iteration in comparison to the fully connected model. A possible explanation for this result is that the convolution kernels are able to extract

features from the input like slopes, peaks and valleys, while a fully connected model is less likely to detect these local dependencies between values.
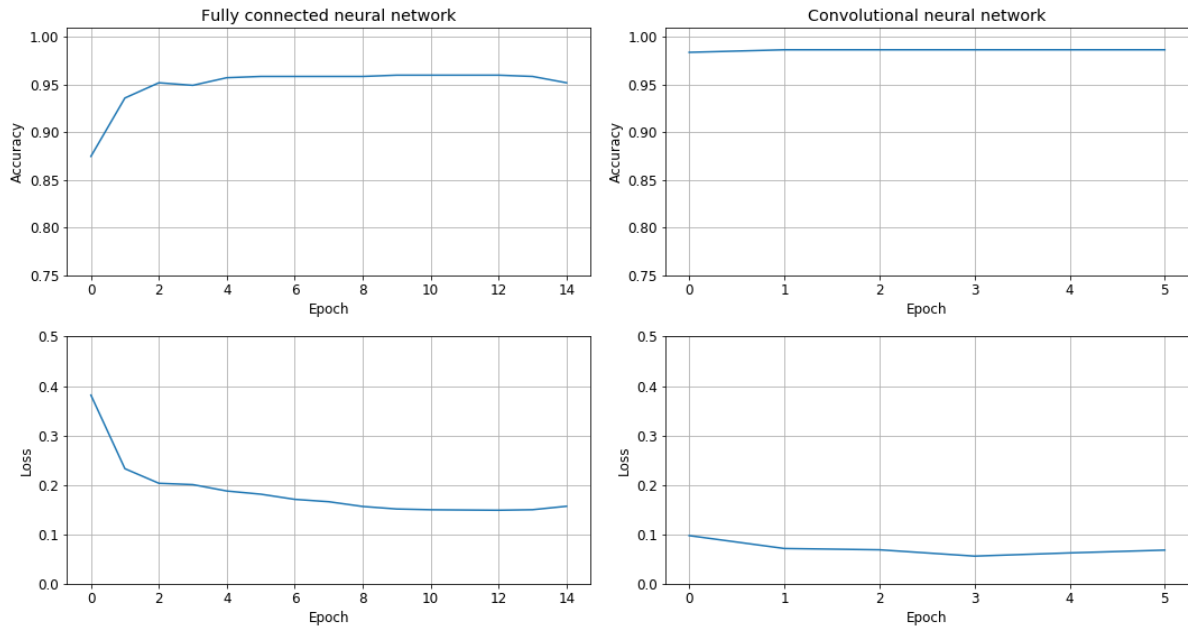
Fig. 6: *Accuracy and loss metric for the two models*

A visual representation of the accuracy of the predictions of both networks is given in Fig 7. As both networks have high accuracy, most points match with the expected values. It can be seen that the convolutional network only wrongly classifies one sample of the testing set, while the fully connected network has worse performance.
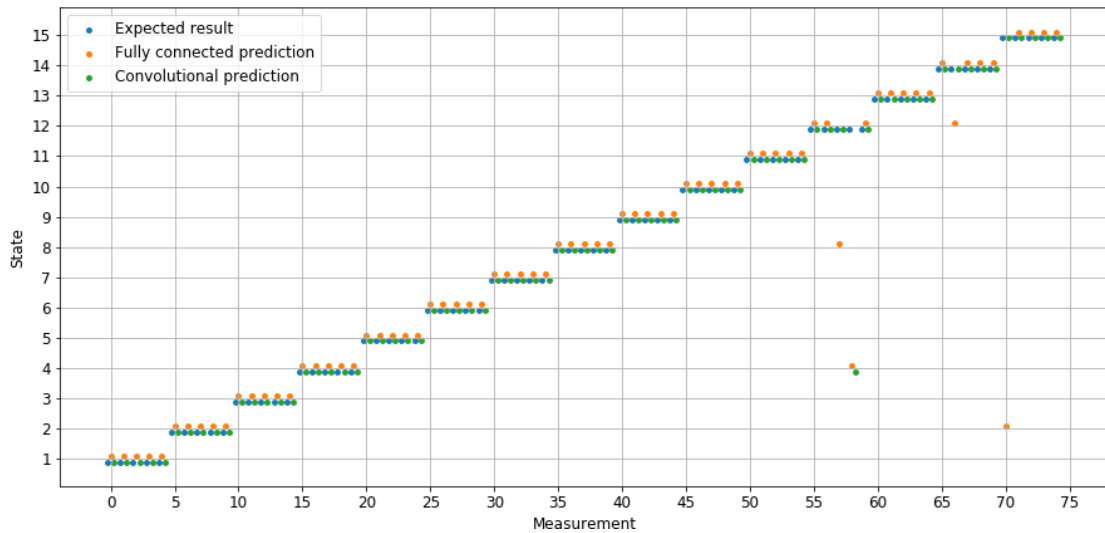
Fig. 7: *Predictions of the different models for the samples in the test set*

Another interesting observation is that the wrong predictions are not close to the actual result. This could indicate that subsequent states do not show a straightforward evolution, meaning that states are highly unique and not closely related. This could prove to be a problem when deploying these models in real world environments as the states in that case would lie in

between the learned states and the drastic changes in spectral data might provoke erroneous predictions.

3.1.2 Regression

The performance of the test set for both models is presented in Fig 8 and Fig 9. Graph in Fig. 8 shows the scatter plot mapping the expected value to the predicted value. Graph in Fig 9 draws the boxplot of the predicted values for each one of the states.

In the case of regression, there is almost no performance difference between the fully connected and the convolutional neural network. Both networks achieve similar results in terms of mean squared error. The results currently obtained do not seem useful in practical application. However, an estimation from a regression network could be used in conjunction with other metrics to provide a more accurate assessment of the state of the container.
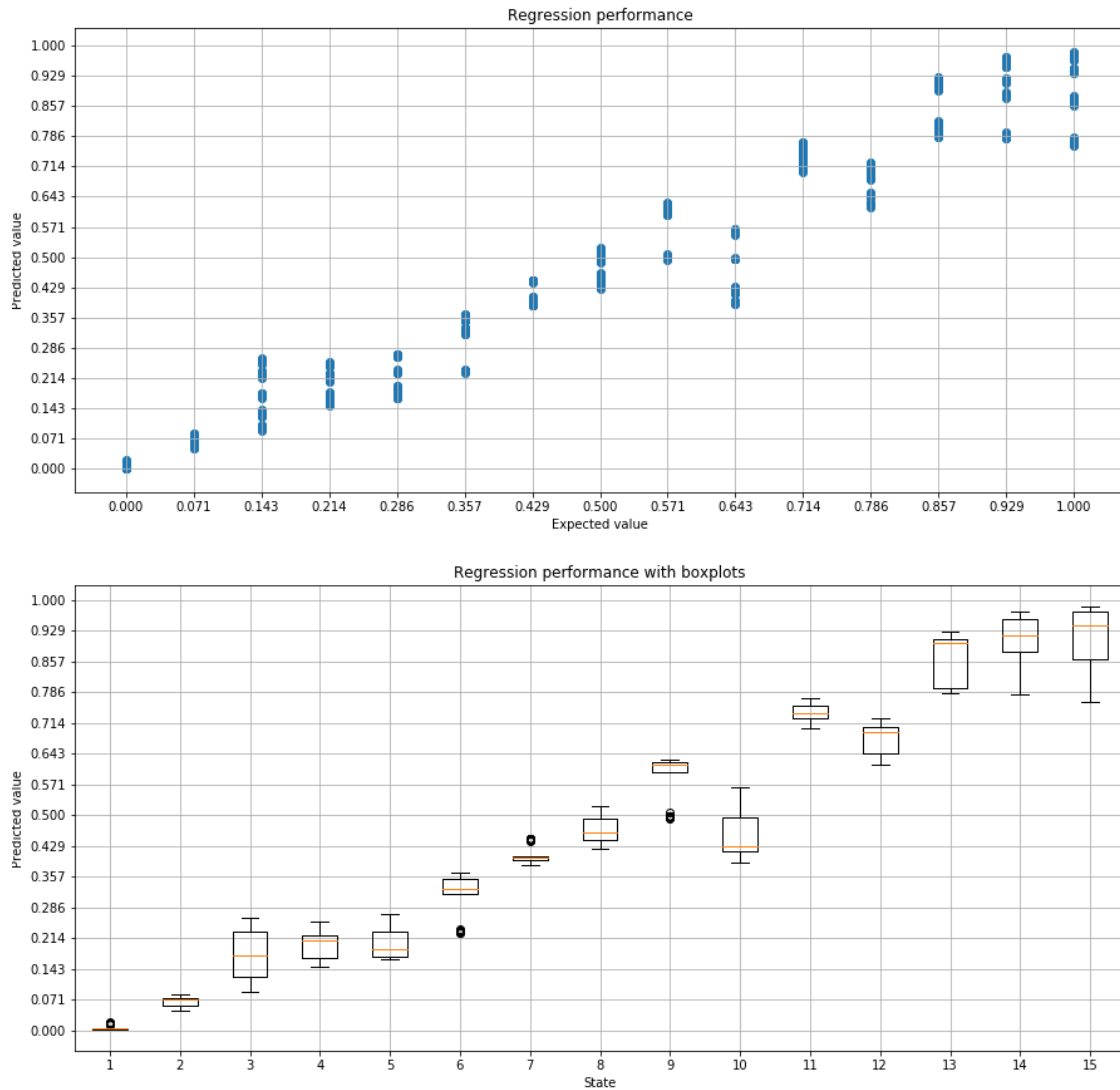
Source: Own
Fig. 8: *Regression performance of the test set for the fully connected neural network*
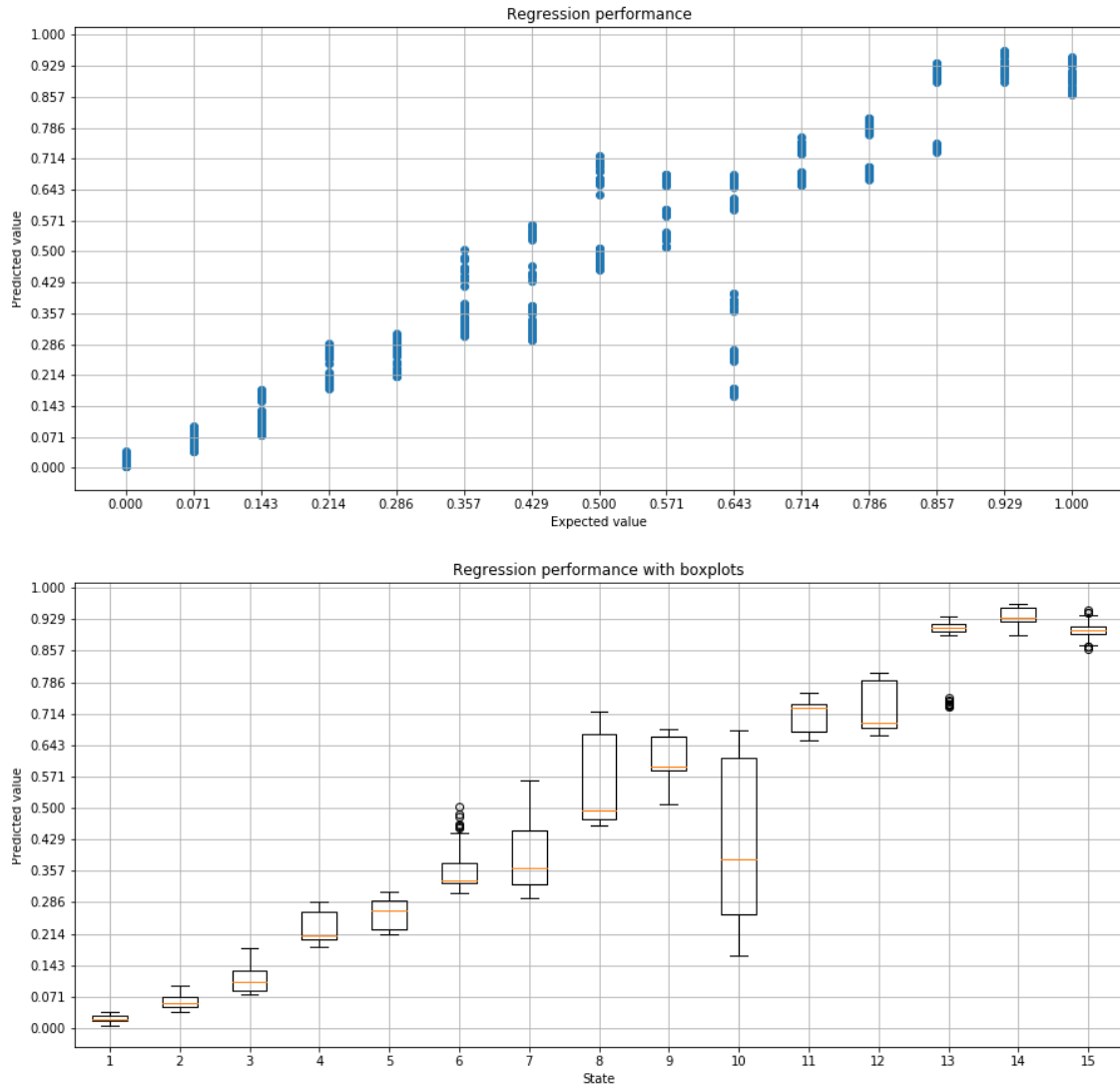
Source: Own

Fig. 9: *Regression performance of the test set for the convolutional neural network*

3.2 Effects of Data Preparation

The accuracy of the fully connected model is shown in Fig 10 with different configurations of data preparation; the results for the convolutional model are similar. Four different configurations were tested, each one with the addition of one extra data preparation step. Starting off without any data preparation, the accuracy of the network is equivalent as randomly guessing the state. With the addition of each of the data preparation measures the accuracy improves accordingly. It can be concluded that each of the data preparation measures explained in section 2.2 have a significant improvement on the performance of a particular model.

Effects of data preparation
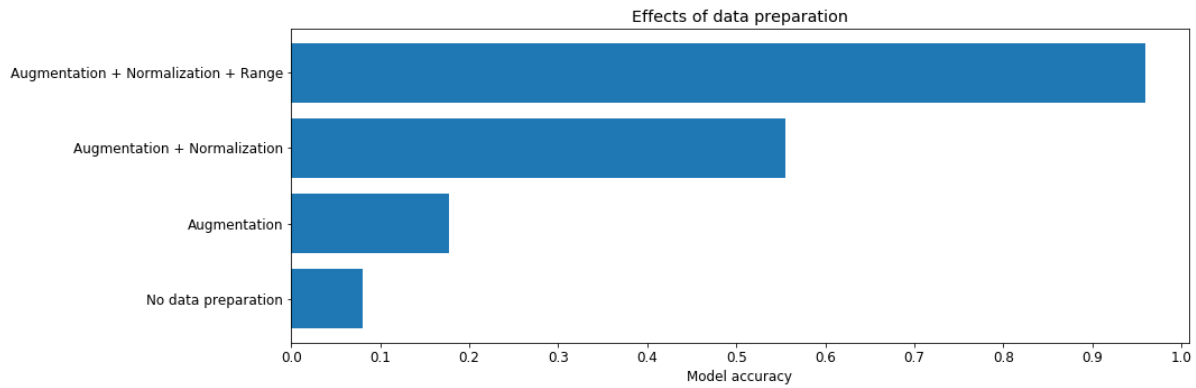
Source: Own

Fig. 10: *Performance benefits gained by using data preparation*

4   Future Work

As the classification spectral data is shown to have very high accuracy, there can be further experimentation with other fuel assembly states. For example, the network can be adapted to classify the exact tube where there is an anomaly by changing the testing setup to have sensors on each axis and to prepare the necessary states.

Further research into the generalization ability of the obtained networks is needed; they need to work in a real world environment where the container state will not exactly be one of the learned states.

Additional work is needed in the case of regression as it shows promise to be able to overcome the limitations with generalization. To accomplish this, the accuracy of the predicted values needs to be refined, possibly by tuning the network parameters or by constructing hybrid models of different regression solutions.

Conclusion

The trained neural networks achieve very high accuracy when classifying spectral data and do not show signs of overfitting.

When using the models to perform regression, the results are less promising. While it is possible to predict a value that is rather close to the expected result, the presence of numerous outliers is worrying. When fine tuning some of the parameters and combining the network with other analysis methods, it is possible that an estimate with sufficient accuracy can be achieved.

Convolutional neural networks are best suited for the analysis of spectral data as they can be built to greater complexity and can recognize local patterns in the data, which certainly is an advantage when considering spectral data. Even though time complexity is greater for the convolutional architectures, the time needed for training is still within reasonable bounds.

When applying different data preparation procedures, the performance of all networks increases accordingly. With the addition of each of the procedures, the overall accuracy of the networks sees a significant improvement.

Acknowledgements

Literature

[1] FISS, D.; SCHMIDT, S.; REINICKE, S.; KRATZSCH, A.: Fundamental R&D Work on Methods for State Monitoring of Transport and Storage Containers for Spent Fuel and Heat-Generating High-Level Radioactive Waste on Prolonged Intermediate Storage. In: *25th International Conference on Nuclear Engineering*. Paper No: ICONE25-67245, V009T15A039. ASME, 2017. ISBN 978-0-7918-5787-8. DOI: 10.1115/ICONE25-67245

[2] BJERRUM, E. J.; GLAHDER, M.; SKOV, T.: Data Augmentation of Spectral Data for Convolutional Neural Network (CNN) Based Deep Chemometrics. In: *ArXiv*. [online]. 2017. Available from WWW: http://arxiv.org/abs/1710.01927

[3] CHOLLET, F. et al.: *Keras*. [online]. 2015. Available from WWW: https://keras.io

[4] ABADI M. et al.: TensorFlow: Large-Scale Machine Learning on Heterogeneous Distributed Systems. Preliminary White Paper. In: *ArXiv Vanity*. [online]. 2015. Available from WWW: https://www.arxiv-vanity.com/papers/1603.04467/

M.Sc. Theo Dedeken

VÝZKUM A VÝVOJ UMĚLÉ NEURONOVÉ SÍTĚ PRO SPEKTRÁLNÍ DATA

Globální výzva k určení stavu obsahu přepravních a skladovacích kontejnerů pro vysoce radioaktivní odpady (sestavy vyhořelého paliva) nabízí jako jedno z možných řešení provedení vibračních analýz a vyhodnocení vibračních odezev pomocí umělých neuronových sítí. U tohoto přístupu byla provedena první šetření. Data o vibracích jsou získána z testovacího nastavení, které modeluje sestavy palivového jaderného úložiště a je převedeno na frekvenční doménu pomocí Fourierovy transformace. Surová spektrální data jsou nejprve připravena normalizací rozšířením dat a omezením frekvenčního rozsahu. Tato opatření mají evidentně významný dopad na celkový výkon neuronových sítí. Za použití plně propojených a konvolučních neuronových sítí se na spektrálních datech provádí klasifikace a regrese. Ukázalo se, že klasifikace je možná s velmi vysokou přesností a regrese má velmi dobré výsledky s možnostmi zlepšení v pozdějších fázích. Konvoluční neuronové sítě se v obou případech jeví jako vynikající.

UNTERSUCHUNG UND ENTWICKLUNG EINES KÜNSTLICHEN NEURALEN NETZES FÜR SPEKTRALE DATEN

Die globale Herausforderung zur Bestimmung des Inhaltes von Transport- und Lagerungscontainern für hoch radioaktive Abfälle (Zusammenstellung von ausgebranntem Brennstoff) bietet als eine der möglichen Lösungen die Durchführung von Vibrationsanalysen und der Auswertung von Vibrationsrückmeldungen mit Hilfe künstlicher Neuronennetze. Bei diesem Ansatz wurden erste Untersuchungen durchgeführt. Die Daten über die Vibrationen wurden aus der Testeinstellung gewonnen, welche die Zusammenstellungen der Kernbrennstofflagerstätte modelliert und an einer Frequenzdomäne mit Hilfe der Fourier-Transformation durchgeführt wird. Die spektralen Rohdaten werden zunächst durch Normalisierung durch Erweiterung der Daten und durch Begrenzung des Frequenzbereichs vorbereitet. Diese Maßnahmen haben eine evident bedeutsame Auswirkung auf die Gesamtleistung der Neuronennetze. Bei der Verwendung voll verbundener und konvolutartiger Neuronennetze werden an den Spektraldaten eine Klassifikation und eine Regression durchgeführt. Es hat sich gezeigt, dass eine Klassifikation mit sehr hoher Genauigkeit möglich ist und die Regression sehr gute Ergebnisse mit Möglichkeiten der Verbesserung in späteren Phasen aufweist. Die konvolutartigen Neuronennetze erweisen sich in beiden Fällen als hervorragend.

BADANIA I ROZWÓJ SZTUCZNEJ SIECI NEURONOWEJ DLA DANYCH WIDMOWYCH

Wystosowano globalny apel do określenia stanu zapasu kontenerów transportowych i magazynowych na odpady wysoce radioaktywne (zestawy wypalonego paliwa). Jednym z możliwych rozwiązań jest wykonanie analiz wibracyjnych oraz ocena działania drgań przy pomocy sztucznych sieci neuronowych. Dla takiego podejścia wykonano pierwsze badania. Dane dotyczące drgań pozyskiwano z ustawienia testowego, które modeluje zestawy składowisk paliwa jądrowego i jest przetworzone na domenę częstotliwości przy pomocy transformacji Fouriera. Surowe dane widmowe są najpierw przygotowane w drodze normalizacji, powiększania zbiorów danych i ograniczenia zakresu drgań. Działania te mają jednoznacznie znaczący wpływ na ogólną wydajność sieci neuronowych. Przy wykorzystaniu w pełni połączonych i splotowych sieci neuronowych na podstawie danych widmowych dokonuje się klasyfikacji i regresji. Okazało się, że klasyfikacja możliwa jest z bardzo dużą dokładnością a regresja osiąga bardzo dobre wyniki z możliwością udoskonalenia na późniejszych etapach. Splotowe sieci neuronowe wydają się w obu przypadkach znakomite.

DEVELOPMENT OF AN INTERACTIVE APPLICATION FOR THE VIRTUAL REALITY

Omar Hussein[1]; **Steffen Härtelt**[2]; **Christian Vogel**[3]; **Alexander Kratzsch**[4]

Hochschule Zittau/Görlitz, IPM Department
Theodor-Körner-Allee 16, 02763, Zittau, Germany
e-mail: [1]omarwanhussein97@gmail.com; [2]s.haertelt@hszg.de; [3]c.vogel@hszg.de;
[4]a.kratzsch@hszg.de

Abstract

This project is an attempt to get expert knowledge of VR technology and have a clear perception of the Linator as an example. The main purposes are helping to gain knowledge of this engine, concepts and mechanism, how its animation works and identify each part (geometries and tasks) by using VR- headset. The idea of this project is to find the way to fully understand this machine and to link the theoretical science to practical reality for educational and industrial purposes in three main steps: Digitalization, Data reparation and acquisition and Animation. The presentation ways depend on the capabilities of both the software and hardware. Thus, this is also an attempt to generalize presentation ways which can be used to apply on other mechanical machines.

Keywords

VR-headset; Linator; IPM; HTC-VIVE Pro; Blender; OTAG; LION Powerblock; CREO; Unity.

Introduction

Linking theoretical science to practical reality is one of the most important issues for educational and industrial purposes.

This paper describes how to have a clear perception of the Linator as an example of other similar applications in mechanical field, find out how to fully understand this machine and investigate the best ways to display such mechanical machines and other applications [1].

VR- headset is a virtual reality headset. This is a head-mounted device that provides virtual reality for the user.

One of the most important topics in the IPM Institute is steam technology and using it to produce efficient power. Therefore, the power block from LION Company which contains Linator is a good application in small scale for educational and industrial purposes.

Linator is a free-piston steam engine, used in electricity and heat generation. As shown in Fig. 1, it uses the pressurized steam to move pistons in each side in fluctuating movement (right and left) to move the rotor which is connected in pistons to generate the magnetic field and then generating electricity, the steam circulate from main holes in condensation part [2]. Linator generates electricity using the same concept of stirling engine to generate magnetic field caused by moving the Squirrel-cage rotor.
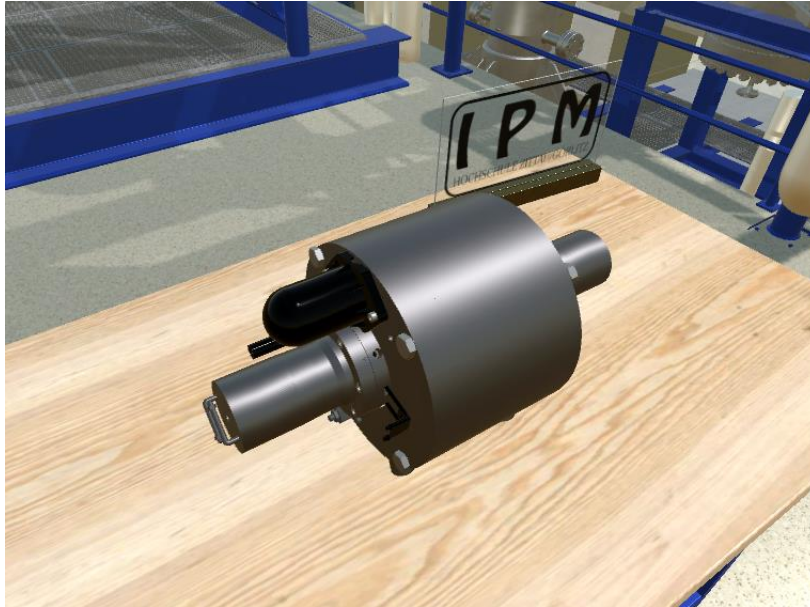
Fig. 1: *3D-model of Linator*

The main purposes of this project are building experience in the virtual reality field (implementation of further applications for the Zittau/Görlitz University of Applied Sciences) and creating a practical application (Linator) by dealing with Linator and all parts as a real experience and creating a suitable environment to understand all information about it in an attractive way.

1 State of the Art

In IPM institute HTC-VIVE Pro is used as a VR-headset technology and Linator is used as an example of mechanical application.

1.1 HTC-VIVE Pro

"VIVE is a virtual reality brand building hardware, software and creative platforms to unleash imaginations from the limits of our world. Sub-millimetre-precise tracking technology from SteamVR. High-fidelity hardware and an ecosystem of innovation from VIVE. Together, they make a superlative experience unlike any other. Jump into the future of art, storytelling, gaming, enterprise and entertainment." [3]

1.2 Linator

Linator is a part of the Powerblock LION [4] produced by "OTAG storm mit wärme" company. Fig. 2 shows the company logo.
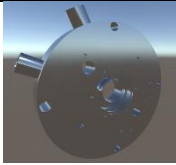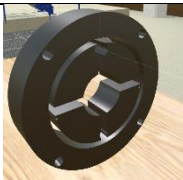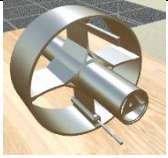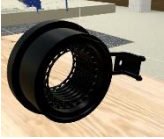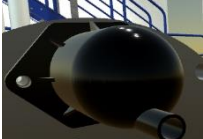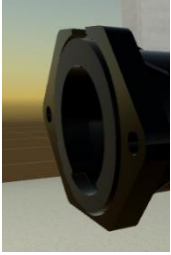
Fig. 2: *Logo of OTAG company*

Table 1 describes the basic parts of Linator and the main function for each part.

Tab. 1: Basic parts of Linator and the main function for each part

No.	Description	Image	No.	Description	Image
1	Housing part This part is one of the biggest parts; in this part the expanded exhaust steam comes out through 2 holes in each side and it works as support of another small parts.		9	Main ring This ring connects the" condenser part" with the "outer chamber" and "Rings of holes"; it has special geometry and holes of bolts to make sure that every parts in the correct location.	
2	Stator part In the middle of the Linator, it consist of permanent magnet on the inner perimeter of outer circle that allows to make a magnetic field to generate the electricity and it consists of a plate of conductor materials with lamination to decrease the eddy current losses.		10	Carbon piston ring It is a small part between the "Inner chamber" and the "Outer chamber" and around the first part in the piston, the basic task for this part is to tight the piston and prevent the steam leakage.	
3	Squirrel-cage rotor By connection in each pistons the rotor move in the linear movement to cut the magnetic field lines and generate current that passes to the specific hole.		11	Circular supporting ring Ring with special geometry works as a supporting ring for the carbon piston ring to prevent steam leakage. It is made of a special kind of brass.	

4	Rubber gasket Rubber ring around the centre of the housing part to prevent any leakage in the steam throw other parts and connect parts without scratching, It has a smooth mesh that allows steam to pass.		12	Electrical cable stand It is a stand that helps the electrical cable to move in flexible way.	
5	Rings of holes This part contains lamination of rings, each ring contains 24 holes to allow the steam to move in a specific place and specific movement, and it also contains two paths to prevent to reach the critical pressure. It consists of lamination to make sure the steam is not free but also it can move without a huge amount of losses and pressure drop. [5]		13	Electrical cable cover This part covers the cable and helps to move freely, also it has a hole in the top for ventilation.	

| 6	Piston		14	Cover gasket	
	The most complicated part in Linator consists of two main parts as shown in the figure, the first part, the cylinder, has smooth outer surface, it inters the high pressure (outer) chamber and has rectangular holes around the outer circle at the end to allow the steam to move to other part at a specific time, these holes work as steam inlet valves and have special radius of curvature to minimize the pressure drop in the steam [6].

This image illustrates the shape of these holes. The second part is the part connected to the rotor and has 3 layers, the first and the second layers are made in a special way as shown from carbon to make sure that piston touches the inner chamber and the last one has a star shape to set all pieces in their correct location. | | | It is made of rubber and it has a special hole to allow the cable to come out from cover. | |
| 7 | Inner chamber | | 15 | Venting part | |
| | This chamber is where steam pushes the piston to move, these are two important things in this part, firstly, it is the smooth part to reduce the friction between the piston and the chamber at the minimum value, secondly, this chamber has 24 holes, which work as steam outlet valves. | | | This part prevents over-pressure by allowing the steam come out from these parts, it is connected with the rotor too by the rod. | |

8	Outer chamber This part works as a cover of "Rings of holes" and the "Inner chamber" part. This part has 4 sections; the first one is considered the outer chamber that allows the steam to enter the engine by two ports and sustain the high pressure, the second and third section cover the parts and the last one is to connect with main ring.				

Source: Own; the figures done by authors using software CREO parametric 3.0 [13]

2 Work Flow

To meet the dead-line of this project, the plan of the work was done in short-term and long-term goals as shown in Fig. 3.
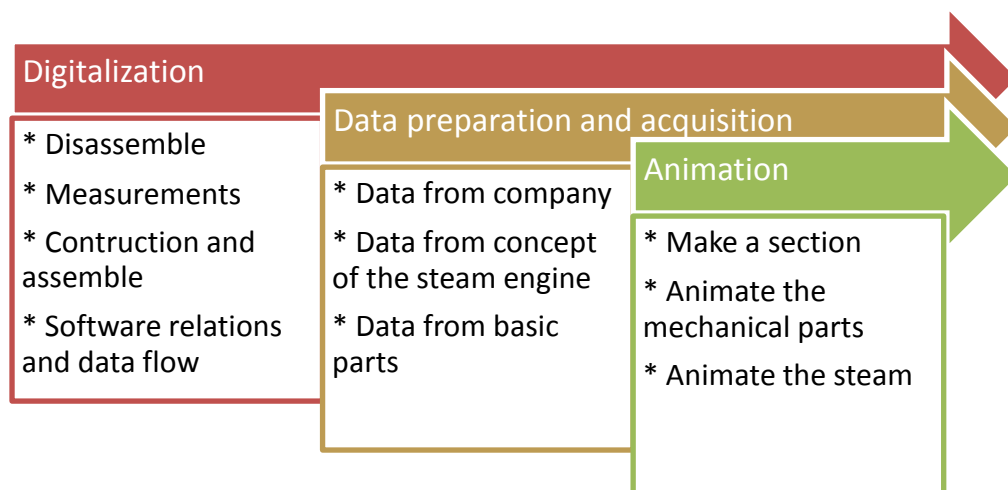
Source: Own
Fig. 3: *Work steps of project*

The sequence of steps illustrates the work flow from the beginning to the end of the working process in this project that concerns to linking theoretical science to practical reality and depends on the presentation ways, the hardware and software that was used and the main purpose of this project.

To reach the goal there was several steps to realize:

- Digitalization
- Data preparation and acquisition
- Animation

2.1 Digitalization

Digitalization is used to convert Linator from the real machine to a virtual reality machine, it is used to make Linator applicable model in SteamVR and other applications. This step is important in this project to be done since that there are no any construction drawings for Linator.

Disassembling the parts of Linator was done by using screw removal tools, as shown in Fig. 4, and hydraulic crane. Linator has about 30 basic parts.

Source: https://www.amazon.it/Stanley-Cassetta-attrezzi-cromata-lucida/dp/B00TBCMLXM
Fig. 4: *Screw removal tools*

A video for disassemble step has been recorded to make sure that every part fits in the correct location, as shown in Fig. 5, and an endoscope was also used to see the small parts inside the engine.

Source: Own
Fig. 5: *Disassemble process*

2.1.1 Measurements

Since there is no any information about the parts and dimensions of these part, Digital Vernier caliper, shown in Fig. 6. is used to measure the dimensions of the parts with high accurate resolution (0.01 mm). Also using 3D-scanner technology helps to measure the smallest dimensions in many complicated parts such as Carbon piston ring.

Fig. 6:   *Digital Vernier caliper*

2.1.2   Construction and Assemble

In parallel with the measurement step, the construction was done by using CREO parametric 3.0 program. This includes the geometries, holes and all links between parts.

The assembly step of the digitalized parts was also done by using CREO parametric 3.0 program with taking into consideration the personal errors and the uncertainty in measurements, as shown in Fig. 7.

Source: Own; screenshot using software CREO parametric 3.0 [13]
Fig. 7:   *Construction and assemble of Linator in CREO parametric 3.0*

2.1.3   Software Relations and Data Flow

To export this model to Unity, it must be in a specific extension (FBX, OBJ, etc.). CREO does not support these extensions, so this is done by using a blender as a mediator to convert the extension from STP to FBX and to make custom section for animation purposes.

Parts and their texture are exported to make animation more realistic. In addition to that, linking VR-headset with Linator model is created by using Unity3D program.

Unity program supports the VR-headset (HTC VIVE PRO) by using the SteamVR Plugin Asset and by writing the scripts (scripting programming language is C#) using Microsoft Visual Studio [9] the interaction between VIVE PRO hardware and the parts on the Linator

(controlling in position, rotation), as shown in Fig. 8. To realize that work, the following software and hardware are used, as shown in Table 2.

Tab. 2: *Software and hardware used*

Software	Hardware
CREO parametric 3.0 (3D-modelling software from PTC company)	HTC-VIVE PRO
Blender 2.79 (3D Computer Graphics Software)	ASUS
Unity 2018.1.7f1 (cross-platform game engine)	Processor: Intel Core i7-7700
SteamVR (virtual reality system)	Graphics: NVIDIA GeForce GTX1080 8GB
VIVEPORT (official app store for the HTC Vive)	Memory: DDR4 SO-DIMM 16GB
Microsoft Visual Studio	

Source: Own

The chart in Fig.8 describes the relations between the software that was used in this project.
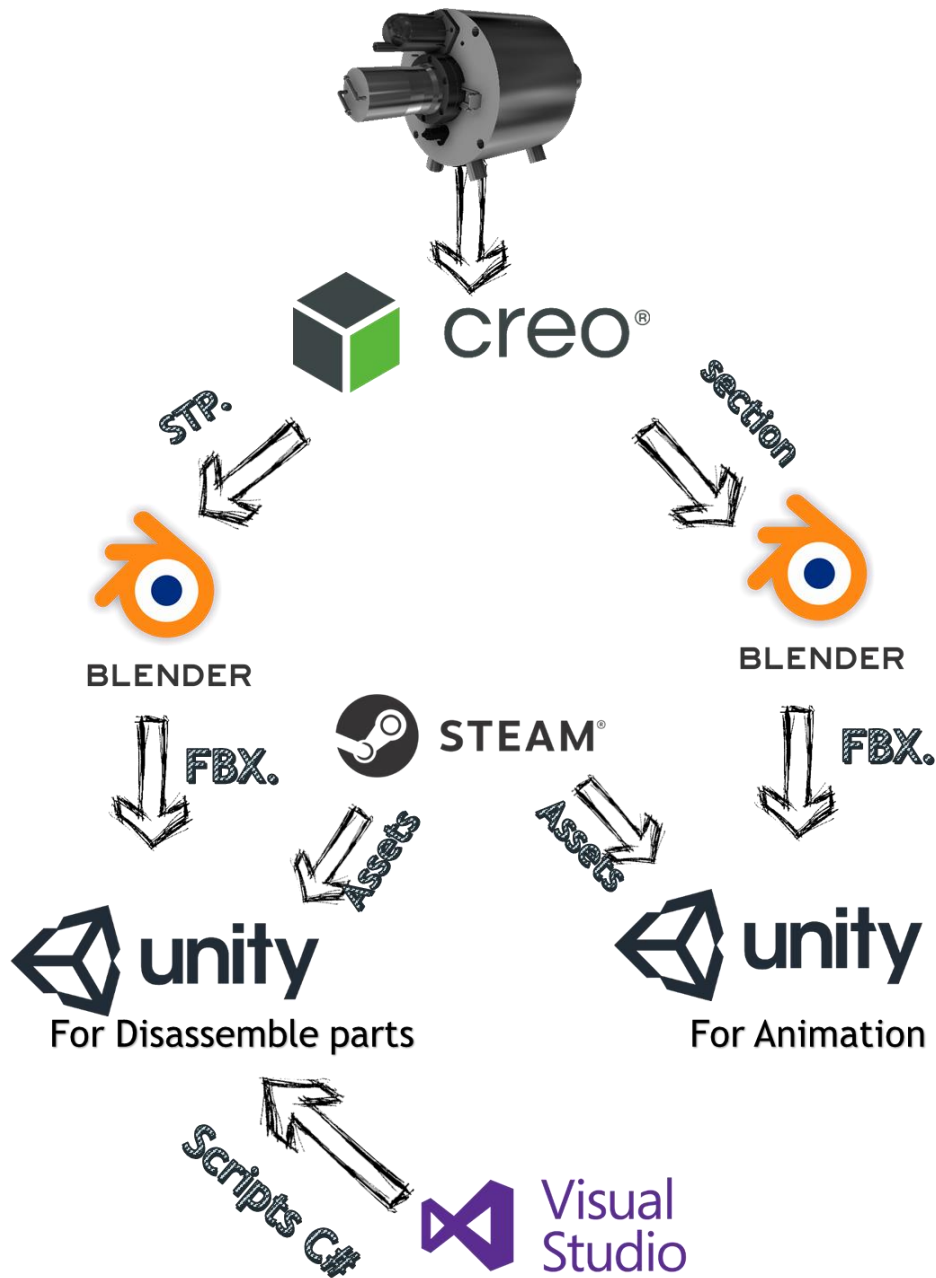
Fig. 8: *The relations between software types*

In addition to drawing and graphics work, scripts were processed in the Unity3D to accomplish this project with all requirements in three ways [8]:

- Using the scripts without any changes, e.g. the player, controller scripts or teleport point.
- Using the scripts with changes to make it suitable for this project like throwable script and start bottoms.
- Creating special scripts for special application like information sound and mesh collider.

2.2   Data Preparation and Acquisition

The purpose of this step is Linator (Tasks, Parts, Materials, etc.) science research by including all theoretical information about Linator in this project. Results are in Table 1.

The data sheets, as shown in Fig. 9, are used from the company, the basic concepts of the free piston steam engine, the shape, materials and assembly of the parts and the holes, valves of these engines [10], [11].

Finally, this research was translated to other languages (German and Arabic) and put in interactive sound in Unity3D to link it with VR-headset.
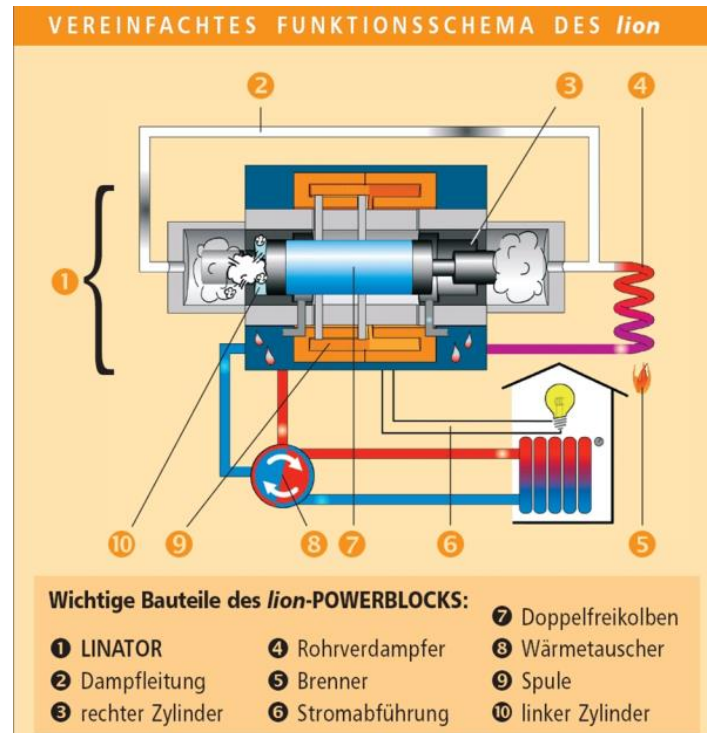
Source: http://www.bhkw-prinz.de/button-energy-bison-powerblock-holzpellets-bhkw/2771
Fig. 9: *Description of how the Linator works*

2.3 Animation

One of the challenges is the animation especially in Unity3D, although it is the best choice to link the digital engine in virtual reality with VR-headset, because Unity3D as a game engine is not suitable for mechanical animation like fluids and relative movement between parts. About 17 different animation for 17 objects were prepared while taking into consideration the relative movement and time delay in each object, as shown in Fig. 10.
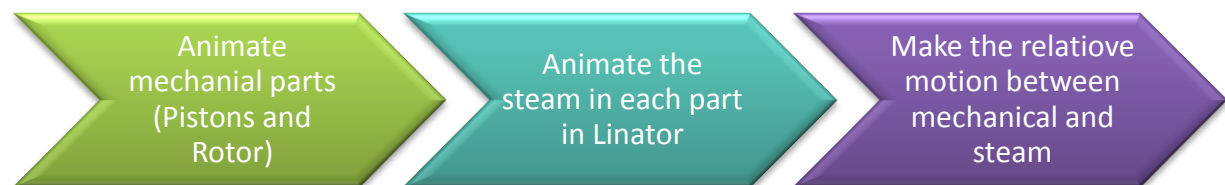
Source: Own
Fig. 10: *Wok steps in the animation*

A clear section is done to demonstrate the inside parts and the main valves, and the movement of the steam in the channels, as shown in Fig. 11.

Source: Own using software Unity 3D [8]
Fig. 11: *Suitable section for animation*

2.3.1 Assumption for Animation and Visualization

- No effect of gravity
- The air resistance (drag) is too large
- No collision between each part
- The connection bolt is static
- The speed in animation is too slow

2.3.2 Presentation Way

Firstly, in front of the first table you can disassemble the parts in Linator by hands of VIVE PRO, control all parts in position and rotation and you can see its geometries, shape and size of the parts and hear interactive voices about information of all parts and tasks of it.

Collider mesh in Unity3D is not suitable for complex mechanical parts and every part has inaccurate meshes that cause the destroying in the assembly. This challenge is solved by trying to make the simplest possible mesh, prevent any collision between each part by writing scripts for that, stop the gravity effect and raise the drag to make the part stable.

The second way is animation about explosion of the Linator to the basic parts to describe the configuration of the parts with each other.

In the third table you will see an animation about how Linator work and the movement of the steam and the parts to clear the holes, input and output valve, tasks of parts and the types of inputs and outputs in Linator, as shown in Fig. 12.
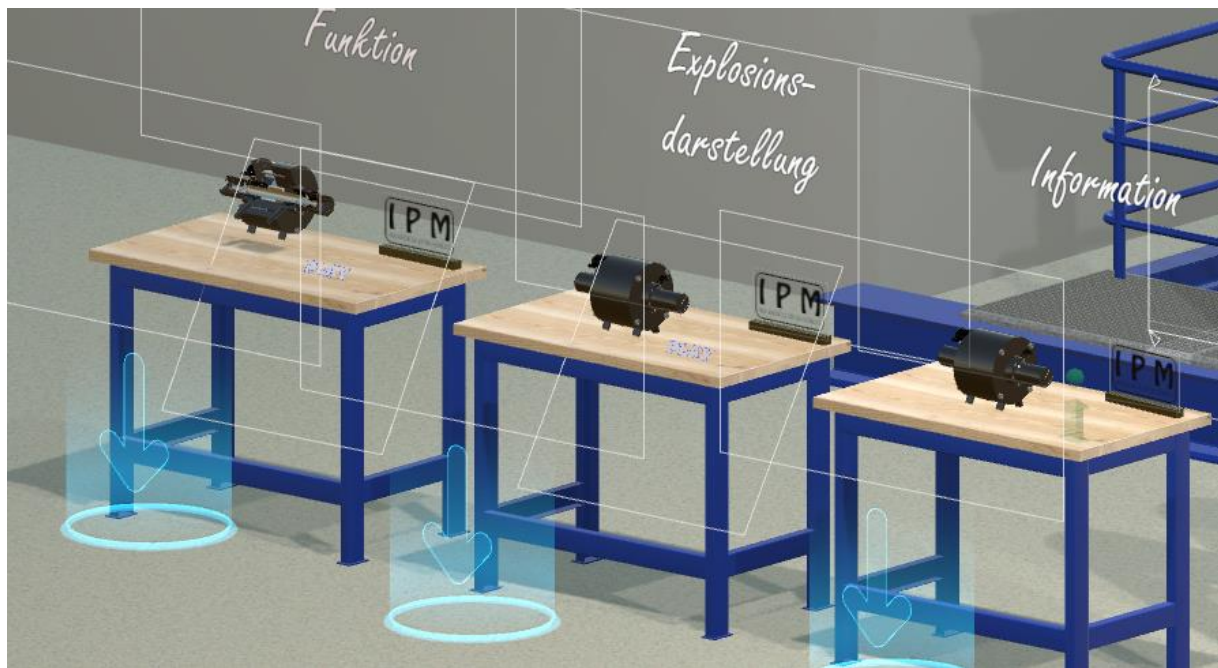
Source: Own using software Unity 3D [8]
Fig. 12: *Presentation ways*

3   Results

Now, the player can make a tour through the laboratory to see the models of the Linator and deal with this engine in three ways; Information: controlling of the parts and seeing the shape and geometry of all parts and listening to the information about any parts in interactive way, Disassemble animation: seeing the animation when the Linator disassemble to the basic parts, Function: seeing the Linator when it works in a special section to display the inlet and outlet valve and the movement of the steam and mechanical parts.

This project is a great application for educational purposes especially in the schools that do not have the possibility to own these mechanical engines or big laboratories. This project contains a huge amount of details in graphics and controlling in all parts.

It can also be used for online courses to reach to the best understanding for this application in the concepts side and physical side (parts, dimensions, tasks and animation, etc.)

On the other hand, it is a nice idea to use it for industrial purposes to simplify the complex processes and display the parts and manufacturing of these parts in interactive tools.

In the marketing, this is one of the most interactive methods to market the products and it helps to display the product in the best way for customers.

Finally, learning through play is not limited for kids, this method gives good understanding in the applications like Linator in an entertaining way [12].

This project helps to understanding all things about Linator and it is the example for application (display, controlling, scripts and animation) that it may be used to make another good applications.

In other words, this project represents a good base to other applications and ideas.

Source: Own
Fig. 13: *Application of the project*

Conclusion

Studying the Linator in this way helps for good understanding of the main concepts in the steam engines and the definition of free piston. Regardless of the limitation of this technology and this method (programs and hardware), it is still effective because the linking between the theoretical sciences to practical reality for many purposes is one of the hardest things to do in this rapidly progressing science. Since this project is the newest idea to link VR technology with mechanical machines, a lot of challenges were faced, e.g. the exporting process and animations especially in steam movement, etc.

The main advantage of this project is the real experience to deal with mechanical machines in a highly interactive way and replace the real machines with virtual machines that do the same work for special purposes. The attraction of this technology is that it allows students to learn in an entertaining way, the possibility to use it in online courses and in marketing field are other advantages of this technology too.

Unity3D and other game engines are not suitable to deal with complex mechanical machines and parts, which makes dealing in unity and other game engines limited and has a lot of problems like the challenges in mesh collider, animations and presentation ways. Also the high cost of this hardware reduces common personal use of this technology.

Finally, this technology can be developed in many ways such as developing the presentation ways to make it more creative and attractive, developing game engines to make it more suitable for mechanical application and choosing other machines with other types of display and control. It is a great technology to use especially in the educational field.

Literature

[1]   SCHROEDER, R.: Learning from virtual reality applications in education. *Virtual Reality*. 1995, Vol. 1, pp. 33–39. DOI: 10.1007/BF02009711

[2]   INNOVATIONSGRUPPE PLUSENERGIE: *Forschungsprogramm Energie in Gebäuden*. [online]. 2012. Available from WWW: https://www.energie-cluster.ch/admin/data/files/file/file/733/01_rolf-moser-27082012-ig-peg4.pdf?lm=1450424226

[3]   VIVE™: *Discover Virtual Reality Beyond Imagination*. [online]. 2020. Available from WWW: https://www.vive.com/

[4]   OTAG: *lion-Powerblock von Otag: das Mikro BHKW fürs Eigenheim*. [online]. 2020. Available from WWW: https://www.heizungsfinder.de/bhkw/hersteller/otag-lion-powerblock

[5]   LÜTHI, A: *Bison Powerblock: Pelletheizung mit linear angetriebenem Dampfmotor*. [online]. 2012. Available from WWW: http://www.holzenergie-symposium.ch/12.HES/%20Pr%8asentationen_12_HES_2012%20pdf/06_Luethi_Bison.pdf

[6]   FRENKEN, K.; NUVOLARI, A.: *The Early Development of the Steam Engine: An Evolutionary Interpretation using Complexity Theory*. [online]. Eindhoven Centre for Innovation Studies, The Netherlands: Technische Universiteit Eindhoven, 2003. Available from WWW: https://pdfs.semanticscholar.org/96df/37a5dfec4effd195085c8dbaa61cb03a0bc2.pdf

[7]   IKZ.de: *Revolutionäre flüssiggasbetriebene BHKW-Technik - Mit dem lion-Powerblock zieht Energieeffizienz in Häuser ein*. [online]. 2009. Available from WWW: https://www.ikz.de/nc/detail/news/detail/revolutionaere-fluessiggasbetriebene-bhkw-technik-mit-dem-lion-powerblock-zieht-energieeffizienz-in/

[8]   UNITY TECHNOLOGIES: *Unity User Manual (2018.2)*. [online]. 2018. Available from WWW: https://docs.unity3d.com/Manual/index.html

[9]   MICROSOFT: *C# documentation*. [online]. 2020. Available from WWW: https://docs.microsoft.com/en-us/dotnet/csharp/

[10]   BHKW-Infothek: *OTAG ist Geschichte, es lebe die „lion energy"*. [online]. 2012. Available from WWW: https://www.bhkw-infothek.de/nachrichten/7581/2012-03-29-otag-ist-geschichte-es-lebe-die-„lion-energy/

[11]   MILITAR, J. G.; ORTWEIN, A.; SENORIO, S. M.; SCHADE, J.: Potential and Demand for Energy from Biomass by Thermo-chemical Conversion in the Province of Antique, Philippines – Part 1, Biomass Availability Analysis. *Philippine Journal of Science*. 2014, Vol. 143, Issue 2, pp. 137–145. ISSN 0031-7683. Available from WWW: http://philjournalsci.dost.gov.ph/home-1/41-vol-143-no-2-december-2014/517-potential-and-demand-for-energy-from-biomass-by-thermo-chemical-conversion-in-the-province-of-antique-philippines-part-1-biomass-availability-analysis

[12]   ROUSSOU, M.; OLIVER, M.; SLATER, M.: The virtual playground: an educational virtual reality environment for evaluating interactivity and conceptual learning. *Virtual Reality*. 2006, Vol. 10, pp. 227–240. DOI: 10.1007/s10055-006-0035-5

[13]   PTC: *Creo Parametric 3D Modeling Software*. [online]. 2020. [accessed 2020-02-18]. Available from WWW: https://www.ptc.com/en/products/cad/creo/parametric

Ing. Omar Hussein; Steffen Härtelt; Ing. Christian Vogel; Prof. Dr.-Ing. Alexander Kratzsch

Vývoj interaktivní aplikace pro virtuální realitu

Tento projekt je pokusem získat odborné znalosti o technologii VR na příkladu Linatoru. Hlavním účelem je pomoci získat znalosti o tomto motoru, konceptech a mechanismech, o fungování animace a identifikovat každou část (geometrii a úkoly) pomocí VR headsetu. Záměrem tohoto projektu je najít způsob, jak plně porozumět tomuto stroji a propojit teoretickou vědu s praktickou realitou pro vzdělávací a průmyslové účely ve třech hlavních krocích: Digitalizace, Oprava a získávání dat a Animace. Prezentační způsoby závisí na schopnostech softwaru a hardwaru. Jedná se tedy také o pokus o zobecnění způsobů prezentace, které lze aplikovat I na jiné mechanické stroje.

Die Entwicklung einer interaktiven Applikation für die virtuelle Realität

Dieses Projekt ist ein Versuch, am Beispiel von Linator fachliche Kenntnisse über die Technologie der virtuellen Realität (VR) er erlangen. Das Hauptziel besteht in der Hilfe bei der Erlangung von Kenntnissen über diesen Motor, die Konzepte und Mechanismen und über das Funktionieren der Animation sowie bei der Identifizierung eines jeden Teils (Geometrie und Aufgaben) mit Hilfe eines VR-Headsets. Die Absicht dieses Projektes ist es, eine Art und Weise zu finden, wie man diese Maschine vollends versteht und die theoretische Wissenschaft mit der praktischen Realität für bildende und industrielle Zwecke zu verknüpfen. Dies soll in drei Schritten geschehen: Digitalisierung, Korrektur und Erlangung von Daten und der Animation. Die Art der Präsentation hängt von den Fähigkeiten von Hardware und Software ab. Es handelt sich also auch um den Versuch um Verallgemeinerung der Arten und Weisen der Präsentation, welche man auch auf andere mechanische Geräte anwenden kann.

Rozwój interaktywnej aplikacji do rzeczywistości wirtualnej

Niniejszy projekt stanowi próbę pozyskania specjalistycznej wiedzy nt. technologii VR (Virtual reality) na przykładzie Linatora. Głównym celem jest pozyskanie wiedzy o tym silniku, koncepcjach i mechanizmach, o funkcjonowaniu animacji oraz zidentyfikowanie każdej części (geometrii i zadań) przy pomocy headset'a VR. Celem tego projektu jest znalezienie sposobu, w jaki można w pełni zrozumieć tę maszynę i połączyć wiedzę teoretyczną z praktyczną rzeczywistością w celach edukacyjnych i przemysłowych w trzech głównych krokach: Digitalizacja, Naprawa i pozyskiwanie danych oraz Animacja. Sposoby prezentacji zależne są od możliwości oprogramowania i sprzętu komputerowego. Dotyczy to więc także próby uogólnienia sposobów prezentacji, które można zastosować także dla innych maszyn mechanicznych.

MODEL OF A LINEAR MOTOR MECHANICAL LOAD

Martin Pustka[1]; **Zdeněk Braier**
VÚTS, a.s., Measurement Department,
Svárovská 619, Liberec XI – Růžodol I, 460 01 Liberec, Czech Republic
e-mail: [1]martin.pustka@vuts.cz

Abstract

The residual vibrations originating from a finite stiffness of the motion control system influence the positioning accuracy of machine working members. This paper deals with the dynamic behavior modelling of a motor load composed of seismic mass supported by two flat springs. Two linear models presented in the paper comprise a continuous model based on the prismatic beam bending vibration theory with appropriated boundary conditions and a discrete model with lumped parameters and a single degree of freedom. Both models were used to simulate the motion of oscillating system with various displacement laws and the results were compared with experimental data measured on a real system.

Keywords

Mechanical vibration; Equivalent model; Damping; Frequency response; Time response.

Introduction

The production machines and machine tools with linear drives produce residual vibrations, which unfavorably influence the positioning accuracy of working members. The spurious vibrations originate from a finite stiffness of the linear motor-working member system. To increase the positioning accuracy special control methods as input shaping, load model (SEM) or controllers with inverse dynamics are employed [1].

The thesis [2] introduces a theoretical and experimental analysis of linear motor loaded on its output by a flexibly mounted mass. The secondary load system consists of a seismic mass m supported by two flat steel springs with rectangular cross-section $b_0 \times h$ and length L (Fig. 1). The mass m can move only in the direction of motor slider without rotation about a normal axis.
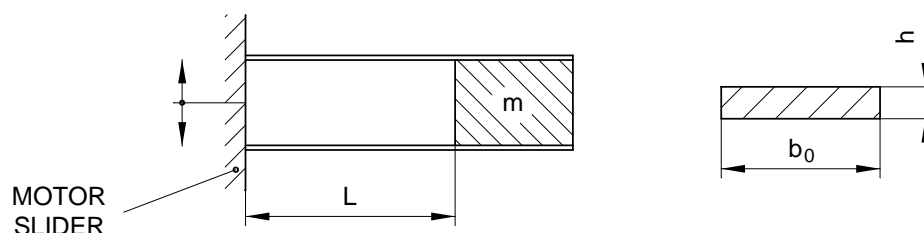
Source: Own
Fig. 1:   *Design of dynamic mechanical load system (left), flat spring cross-section (right)*

This mechanical load system was used to verify various control algorithms and methods for measurement and evaluation of motor and mass kinematic quantities. One of the problems was the substitution of the secondary oscillating system by a suitable mechanical model and its control circuit implementation. Several simple models were successively created, in this paper two possible methods of linear modelling by means of a distributed parameter system

and a single mass system with lumped parameters are presented. Two parallel springs are substituted by one spring with a thickness $b = 2b_0$. The calculated frequency response functions and time responses are compared with experimental data.

1 Distributed Parameter Model (Continuous Model)

The flexible mounted mass is modelled as a laterally vibrating cantilever beam with a discrete mass at the free end (Fig. 2). The system is excited by a base motion of the clamped end [3].
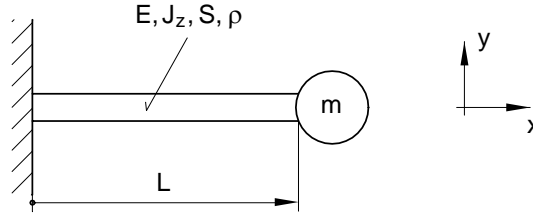
Source: Own
Fig. 2: *Distributed parameter model*

The general equation of motion for the lateral vibration of a uniform beam is [4]

$$\frac{\partial^2 y}{\partial t^2} + \frac{EJ_Z}{\rho S}\frac{\partial^4 y}{\partial x^4} = 0,\tag{1}$$

where E is the Young's modulus, $J_Z = \frac{bh^3}{12}$ is the area moment of inertia of the beam cross-section, ρ the density and $S = bh$ is the cross-section area. We consider the steady-state solution in the form

$$y(x,t) = [C_1 \cosh \beta x + C_2 \sinh \beta x + C_3 \cos \beta x + C_4 \sin \beta x]e^{j\omega t} = y(x)e^{j\omega t},\tag{2}$$

where C_i are unknown amplitudes, ω is angular frequency and β is normalized frequency. The system is excited by a harmonic displacement $y_0 e^{j\omega t}$ at the clamped end $x = 0$, the rigid mass m moves in direction y without rotation at the free end $x = L$. The boundary conditions have then a form

$$y(0) = y_0, \frac{\partial y}{\partial x}(0) = 0, \frac{\partial y}{\partial x}(L) = 0, \frac{\partial^3 y}{\partial x^3}(L) = -\frac{\omega^2 m}{EJ_Z}y(L).\tag{3}$$

Substituting the solution (2) into boundary conditions (3) we obtain the relations for unknown coefficients C_i

$$C_1 = \frac{y_0}{2}\frac{1 - \cosh\beta L \cos\beta L - \sinh\beta L \sin\beta L - \frac{2}{\beta L}\frac{\rho SL}{m}\cosh\beta L \sin\beta L}{1 - \cosh\beta L \cos\beta L - \frac{1}{\beta L}\frac{\rho SL}{m}(\cosh\beta L \sin\beta L + \cos\beta L \sinh\beta L)},$$

$$C_2 = \frac{y_0}{2}\frac{\cosh\beta L \sin\beta L + \cos\beta L \sinh\beta L + \frac{2}{\beta L}\frac{\rho SL}{m}\sinh\beta L \sin\beta L}{1 - \cosh\beta L \cos\beta L - \frac{1}{\beta L}\frac{\rho SL}{m}(\cosh\beta L \sin\beta L + \cos\beta L \sinh\beta L)},\tag{4}$$

$$C_3 = -C_1 + y_0, C_4 = -C_2.$$

The denominator in expressions (4) is the frequency equation (5)

$$1 - \cosh\beta L \cos\beta L - \frac{1}{\beta L}\frac{\rho SL}{m}(\cosh\beta L \sin\beta L + \cos\beta L \sinh\beta L) = 0\tag{5}$$

with roots βL. The eigenfrequencies of bending vibration can easily be obtained from equation

$$f_{01} = \frac{(\beta L)^2}{2\pi L^2} \sqrt{\frac{EJ_z}{\rho S}}.$$

(6)

The frequency response function of the system (a ratio between displacements at the free and clamped end) is calculated from Eqs. (2) and (4) as

$$H(\omega) = \frac{y(L)}{y_0}(\omega).$$

(7)

Using the inverse Fourier transform we get the impulse response function $h(t) = \text{FFT}^{-1}H(\omega)$. The displacement at the free end is defined by a convolution of base motion $y(0,t)$ and impulse function $h(t)$

$$y(L,t) = y(0,t) * h(t).$$

(8)

2 Lumped Parameter Model (Discrete Model)

The flexible mounted mass is approximated by a discrete mass-spring-damper system (Fig. 3). This system is excited by a base motion y_1 and has a single degree of freedom.
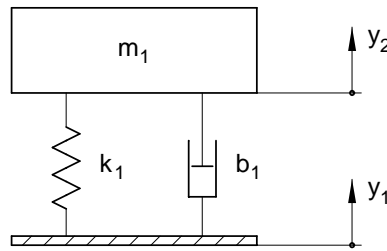
Source: Own

Fig. 3: *Lumped parameter model*

The equation of motion of a system excited through elastic support is

$$m_1 \ddot{y}_2(t) + b_1 \dot{y}_2(t) + k_1 y_2(t) = b_1 \dot{y}_1(t) + k_1 y_1(t)$$

(9)

and model parameters are given by [4]

$$m_1 = m + m_R, \; k_1 = \frac{12EJ_z}{L^3}, \; b_1 = 2\xi\sqrt{m_1 k_1},$$

(10)

where $m_R = \frac{13}{35}\rho SL$ is the reduced mass of flat spring and ξ is the viscous damping ratio. The system eigenfrequency is expressed as

$$f_{02} = \frac{1}{2\pi} \sqrt{\frac{k_1}{m_1}}.$$

(11)

The frequency response function $H(\omega)$ can be obtained by substituting $y_i(t) = y_i e^{j\omega t}$ for y_i into Eq. (9). The displacement time course $y_2(t)$ is a solution of wave equation (9) with exciting waveform $y_1(t)$ and its derivative $\dot{y}_1(t)$ on the right-hand side.

3 Simulation Results

The theoretical models were used to simulate the seismic mass motion excited by motor slider. The calculation was carried out using real values of mass $m = 0.56$ kg, supported by two flat steel springs of length $L = 0.04$ m and cross-section area $b_0 \times h = 25 \times 0.4$ mm^2. The system eigenfrequency $f_m = 17.5$ Hz and the viscous damping ratio $\xi = 0.005$ were determined from measured transient vibration excited by a force pulse [5]. As the spring mounting at both ends is not perfectly stiff, the constants E and k_1 were substituted by effective values E^* and k_1',

$$E^* = E(1 + \mathrm{j}\eta)\left(\frac{f_m}{f_{01}}\right)^2, \; k_1' = k_1\left(\frac{f_m}{f_{02}}\right)^2, \tag{12}$$

where the original eigenfrequencies f_{01}, f_{02} are given by (6) and (11) and $\eta = 2\xi$ is the hysteretic damping loss factor. The model viscoelastic behavior is described by the complex Young's modulus E^*.

Fig. 4 shows the frequency response function of the continuous model calculated using Eq. (7). The maximum of amplitude characteristics corresponds to the lowest bending eigenfrequency. The frequency response function of the discrete model calculated using Eq. (9) is virtually identical in the given frequency range.
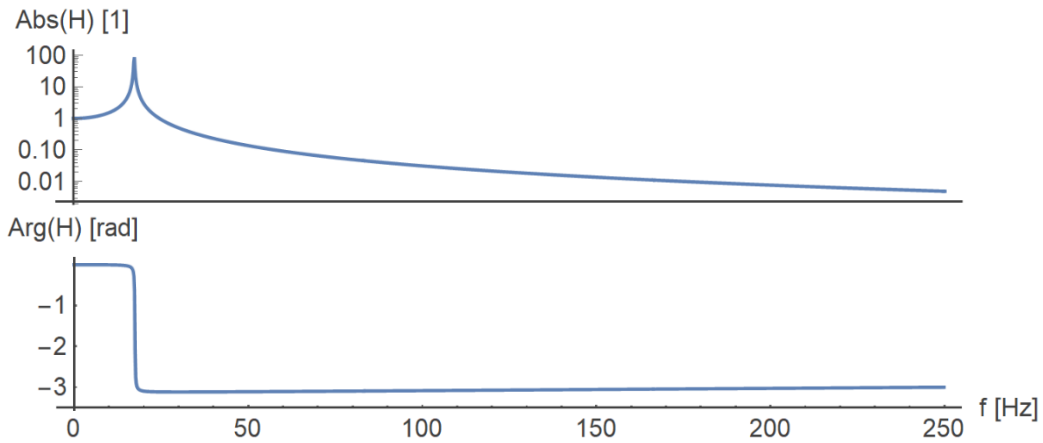
Source: Own
Fig. 4: *Frequency response function of the oscillating system*

The time response of oscillating system was successively assessed for various motor displacement laws. Fig. 5 (top) depicts an example of three periods of measured slider displacement $y(0, t)$, which corresponds to the displacement law labeled F1. The seismic mass displacement $y(L, t)$ calculated using Eq. (8) is shown in Fig. 5 (bottom).

The assessment of oscillating system vibrations from diagrams shown in Fig. 5 is not illustrative. Therefore, the relative seismic mass displacement with respect to slider displacement $\Delta y = y(L) - y(0)$ was further evaluated. Fig. 6 depicts the relative displacements of continuous (steady-state) model (top), of discrete model ($\Delta y = y_2 - y_1$) (middle) and the measured course for comparison (bottom). The response of the continuous model calculated using convolution (8) has three periods of steady-state vibrations, the solution of the discrete model from Eq. (9) includes also the initial transient state. After the transient motion disappears (approximately from the third period) the results of both models are in good agreement as is clear from Fig. 7.
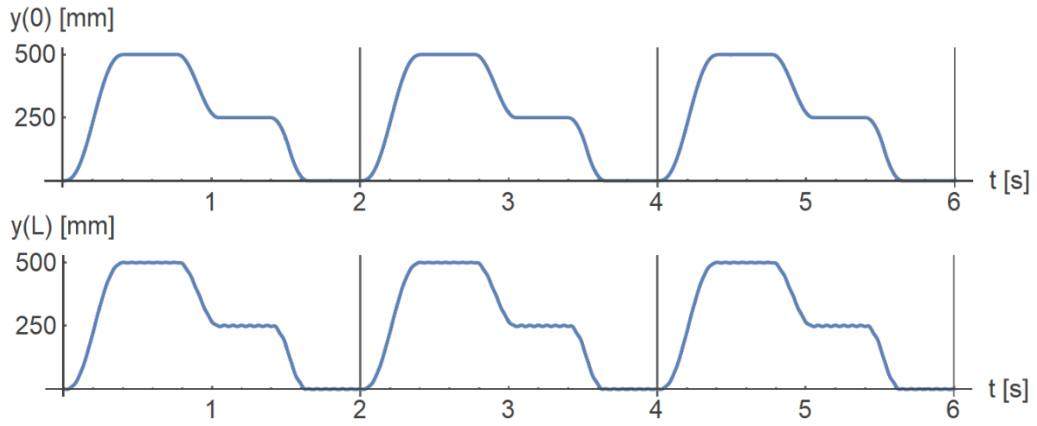
Fig. 5: *Measured motor slider displacement (top) and calculated displacement of oscillating system (bottom) for displacement law F1*
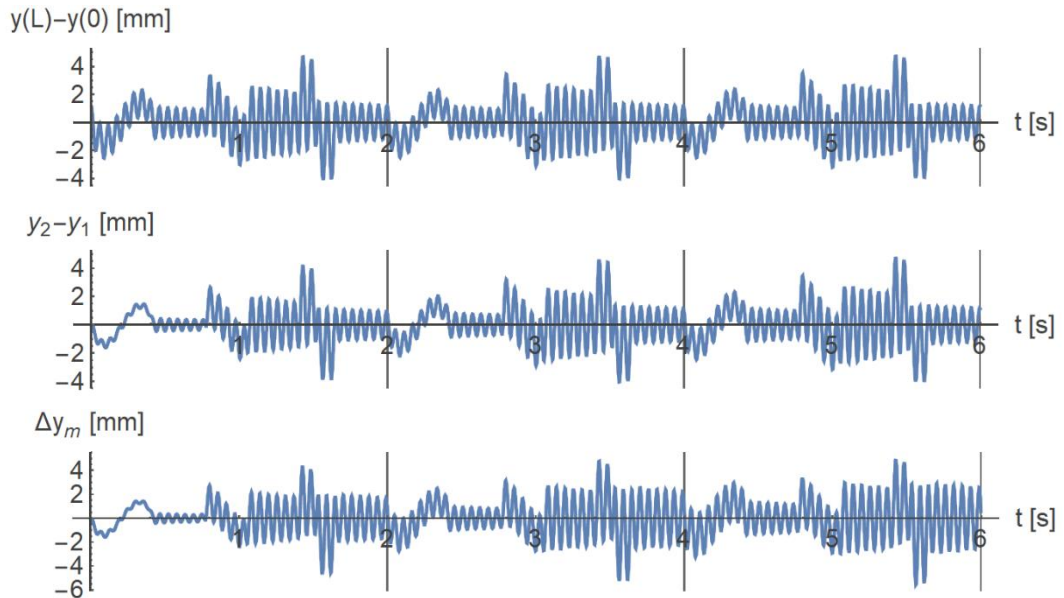
Fig. 6: *Relative displacement of oscillating system (top – continuous model, middle – discrete model, bottom – measured time course)*
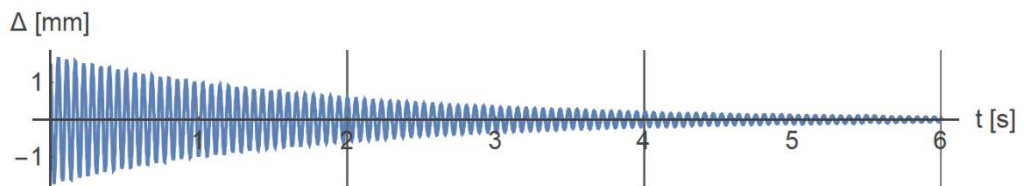
Fig. 7: *Difference of relative displacements Δy of continuous and discrete model*

The comparison of one period of continuous model steady-state vibrations (red) with measured time course (green) is shown in Fig. 8. The theoretical time course fairly coincides with measurement, only in the last part of the cycle (motor at standstill) the calculated vibrations have approximately half amplitude. The main reason for this difference are phase shifts of summands in relative displacement.
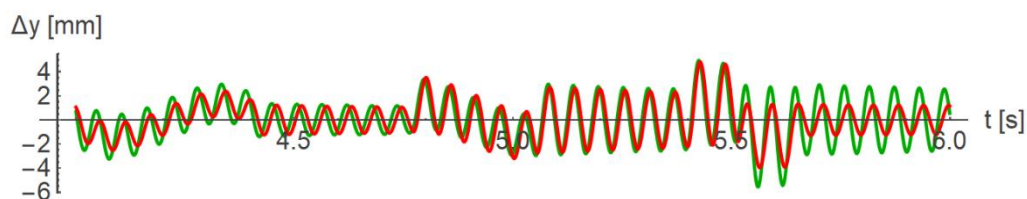
Source: Own

Fig. 8: *Relative displacement of oscillating system (red – discrete model, green – measured time course)*

Conclusion

Several linear models of oscillating system were created within the design process of control algorithm for linear motor loaded on its output by flexibly mounted mass. In the paper the continuous model based on the prismatic beam bending vibration theory and the discrete lumped parameter model with a single degree of freedom were introduced.

Both models were used to simulate the motion of oscillating system with various displacement laws and the results were compared with experimental data. The differences between model results and measured values are small in terms of control requirements. After model implementation into control algorithm and using the input shaping method almost two orders of magnitude suppression of unwanted vibrations was achieved [6].

Acknowledgements

Literature

[1] JIRÁSKO, P. et al.: *Special mechanisms and their drives. Part III.* VÚTS, a.s., Liberec, 2018. ISBN 978-80-87184-86-8.

[2] BRAIER, Z.: *Analýza chování a měření lineárního motoru s dynamicky uloženou kmitající hmotou na pružinách.* Ph.D. Thesis. Faculty of Mechatronics, Informatics and Interdisciplinary Studies, Technical University of Liberec, 2019.

[3] PUSTKA, M.; ERHART, J.; MOKRÝ, P.: Vibration control using piezoelectric bimorphs connected to negative capacitance circuits. *Advances in Applied Ceramics.* 2010, Vol. 109, Issue 3, pp. 180-183. DOI: 10.1179/174367509X12447975734113

[4] BREPTA, R.; PŮST, L.; TUREK, F.: *Mechanické kmitání.* Sobotáles, Praha, 1994. ISBN 80-901684-8-5.

[5] EWINS, D. J.: *Modal Testing: Theory, Practice and Application.* Research Studies Press, Baldock, 2000. ISBN-10: 0863802184. ISBN-13: 9780863802188.

[6] BRAIER, Z.; ŠIDLOF, P.; FIŠER, P.: Measurement, evaluation and comparison of positioning accuracy and other SGT linear motor quantities. In: *14th International Conference Mechatronic Systems and Materials MSM 2018.* AIP, 2018. DOI: 10.1063/1.5066470

Ing. Martin Pustka, Ph.D.; Ing. Zdeněk Braier

MODEL MECHANICKÉ ZÁTĚŽE LINEÁRNÍHO MOTORU

Residuální kmitání způsobené poddajnostmi v soustavě lineárního pohonu a zátěže ovlivňuje přesnost výsledné polohy pracovního členu. Článek se zabývá modelováním dynamického chování zátěže tvořené seismickou hmotou uloženou na dvou plochých pružinách. Uvedeny jsou dva lineární modely – spojitý model odvozený na základě teorie ohybových kmitů prizmatického nosníku s odpovídajícími okrajovými podmínkami a diskrétní model se soustředěnými prvky o jednom stupni volnosti. Oba modely byly použity k simulaci pohybu připojené soustavy pro různé průběhy zdvihových funkcí motoru a porovnány s průběhy naměřenými na reálné soustavě.

MODELL DER MECHANISCHEN BELASTUNG DES LINEARMOTORS

Die Residualschwingungen, die von einer im System des Linearmotors und der Belastung auftretenden Nachgiebigkeit verursacht werden, beeinflussen die Zielpositionsgenauigkeit des Arbeitsglieds. Der Artikel befasst sich mit der Modellierung des dynamischen Motorverhaltens bei einer Belastung, die von einer über zwei Blattfedern gelagerten seismischen Masse erzeugt wird. Es werden zwei Linearmodelle angegeben, ein kontinuierliches Modell, das auf der Basis der Biegeschwingungstheorie vom prismatischen Balken mit entsprechender Randbedingungen abgeleitet ist, und ein diskretes Modell mit konzentrierten Parametern und einem Spielraumgrad. Beide Modelle wurden für eine Simulation der Strukturbewegung bei verschiedenen Motorbewegungsgesetzen verwendet und mit den auf dem realen System gemessenen Verläufen verglichen.

MODEL MECHANICZNEJ WYTRZYMAŁOŚCI SILNIKA LINIOWEGO

Drgania resztkowe spowodowane sztywnością układu napędu liniowego oraz obciążenia wpływają na dokładność ostatecznego położenia elementu roboczego. Artykuł poświęcony jest modelowaniu dynamicznego zachowania pod obciążeniem tworzonym przez masę sejsmiczną ułożoną na dwóch płaskich sprężynach. Przedstawiono dwa modele liniowe – model ciągły opracowany na podstawie teorii drgań zginających pręta pryzmatycznego z odpowiednimi warunkami skrajnymi oraz model dyskretny ze skupionymi elementami o jednym stopniu swobody. Oba modele zostaną wykorzystane do symulacji ruchu przyłączonego układu dla różnych przebiegów funkcji skokowej silnika oraz porównane z przebiegami zmierzonymi na rzeczywistym układzie.

LIST OF AUTHORS

Name	E-Mail and Page Number of Contribution	
Yassin Mustafa Ahmed	yassin.ahmed@spu.edu.iq	7
Hameed D. Lafta	hameed.lafta@spu.edu.iq	7
Azhin Abdullah Abdul Rahman	azhinabdullah92@gmail.com	7
Barzan Talib Salih	barzan69@gmail.com	7
Theo Dedeken	theo.dedeken@telenet.be	19
Omar Hussein	omarwanhussein97@gmail.com	31
Steffen Härtelt	s.haertelt@hszg.de	31
Christian Vogel	c.vogel@hszg.de	31
Alexander Kratzsch	a.kratzsch@hszg.de	31
Martin Pustka	martin.pustka@vuts.cz	47
Zdeněk Braier	-	47

GUIDELINES FOR CONTRIBUTORS

Guidelines for contributors are written in the form of a template which is available as a Word document at http://acc-ern.tul.cz/images/journal/ACC_Journal_Template.docx.

Upozornění pro čtenáře

Příspěvky v časopise jsou recenzovány a prošly jazykovou redakcí.

Readers' notice

Contributions in the journal have been reviewed and edited.

Předplatné

Objednávky předplatného přijímá redakce. Cena předplatného za rok je 900,- Kč mimo balné a poštovné. Starší čísla lze objednat do vyčerpání zásob (cena 200,- Kč za kus).

Subscription

Subscription orders must be sent to the editorial office. The price is 40 € a year excluding postage and packaging. It is possible to order older issues only until present supplies are exhausted (8 € an issue).

Časopis ACC JOURNAL vychází třikrát ročně (červen, září, prosinec).
Three issues of ACC JOURNAL are published every year (June, September, December).